

CHALMERS UNIVERSITY OF TECHNOLOGY  
Department of Applied Acoustics and  
Department of Structural Mechanics

Thesis for the  
Degree of  
Master of Science

**Measuring and Analysis  
of  
Pyrotechnic Shock**

John Eriksson  
Mattias Hansson

Supervisors:

Krister Larsson  
Michael Sanderson  
Ulrika Wendt  
Mats Lago

Dept. of Applied Acoustics, CTH  
Dept. of Applied Acoustics, CTH  
Dept. of Structural Mechanics, CTH  
Saab Ericsson Space AB

Examiner:

Wolfgang Kropp  
Ulrika Wendt

Dept. of Applied Acoustics, CTH  
Dept. of Structural Mechanics, CTH

Gothenburg  
September 1999

Report E99-08, 99:9  
ISSN 0283-8338

# Table of contents

<b>1. INTRODUCTION</b>	<b>4</b>
<b>2. HOW PYROTECHNIC SHOCK CAN AFFECT ELECTRONIC COMPONENTS</b>	<b>4</b>
<b>3. PYROSHOCK TESTING</b>	<b>5</b>
3.1 STANDARD SHOCK-TESTING MACHINES	5
3.1.1 <i>Shock machines</i>	5
3.1.2 <i>Electrodynamic Shakers</i>	5
3.1.3 <i>Resonant Fixtures</i>	6
3.1.3.1 General-Purpose Resonant Fixtures	6
3.1.3.2 Full-Scale Tests.	6
3.1.3.3 MIPS (Mechanical Impulse Pyro Shock) Simulator:	6
3.1.3.4 Changing the characteristic of SRS for the MIPS simulator	8
3.1.4 <i>Tuned resonant fixtures</i>	10
3.1.4.1 Resonant Plate (Bending Response)	10
3.1.4.2 Resonant Bar (Longitudinal Response)	11
3.1.5 <i>Tunable Resonant Fixtures with an Adjustable Knee Frequency</i>	12
3.1.5.1 Tunable Resonant Bars	12
3.1.5.2 Tunable Resonant Beams	12
3.2 MEASUREMENT TECHNIQUES	13
3.2.1 <i>Accelerometers</i>	13
3.2.2 <i>Strain gages</i>	14
3.2.3 <i>Laser Doppler vibrometer (LDV)</i>	14
3.3 LOADING	14
3.3.1 <i>Mechanical impacts</i>	15
3.3.1.1 Effect of the type of excitations	15
3.3.1.2 Effect of impact head materials	16
3.3.2 <i>Pyrotechnically impacts</i>	16
3.4 MEASUREMENTS PROBLEMS	17
3.4.1 <i>Accelerometer problems</i>	17
3.4.2 <i>Mass-loading effect</i>	17
<b>4. TECHNIQUE FOR QUANTIFYING PYROSHOCK</b>	<b>18</b>
4.1 THE SHOCK RESPONSE SPECTRUM MODEL (SRS)	18
4.1.1 <i>Damping</i>	19
4.1.2 <i>1/6 Octave bandwidth</i>	20
4.1.3 <i>To plot the Shock Response Spectrum</i>	20
4.1.4 <i>Pyroshock levels</i>	21
4.1.4.1 Advantages and disadvantages of the SRS	22
4.2 ALTERNATIVE METHODS TO QUANTIFYING PYROSHOCK	22
4.2.1 <i>The Fourier and the Energy spectrum</i>	22
4.2.2 <i>Least favourable response (LFR).</i>	23
4.2.3 <i>Shock intensity spectrum based on the Fourier energy spectrum</i>	23
<b>5. ANALYSIS METHODS</b>	<b>23</b>
5.1 SEA	23
5.1.1 <i>SEA formulation</i>	24
5.1.1.1 Dissipation Loss Factor (DLF)	24
5.1.2 <i>Advantages in the use of SEA</i>	25
5.1.3 <i>Disadvantages in the use of SEA</i>	25
5.1.4 <i>AUTOSEA2</i>	26
5.2 ANALYTICAL METHODS	26
5.2.1 <i>Advantages and disadvantages</i>	28
5.3 FEM	28
5.3.1 <i>Introduction</i>	28
5.3.2 <i>FEM explicit versus implicit solutions</i>	29
5.3.3 <i>Mode superposition</i>	30
<b>6. TEST FACILITY DESCRIPTION</b>	<b>31</b>

6.1	PYROSHOCK TEST DESCRIPTION	31
6.1.1	<i>Statement of the problem.</i>	31
6.1.2	<i>Test facility description</i>	31
6.2	DATA ACQUISITION	32
6.2.1	<i>Test setup</i>	32
6.2.2	<i>Test facility description</i>	33
6.2.3	<i>Accelerometers</i>	34
6.2.4	<i>The amplifier</i>	35
6.2.5	<i>Lecroy oscilloscope</i>	35
6.2.6	<i>Interface card</i>	35
6.2.7	<i>Interface card software</i>	35
6.2.8	<i>Scangraph</i>	35
6.2.9	<i>SRS-program</i>	35
<b>7.</b>	<b>MEASUREMENT OF PYROTECHNIC SHOCK</b>	<b>36</b>
7.1	REPEATABILITY	36
7.2	POSITIVE AND NEGATIVE SRS'S	37
7.3	CHANGING THE CHARACTERISTICS OF SRS	38
7.3.1	<i>Effect of changing of the drop angle</i>	38
7.3.2	<i>Effect of changing the hammerweight</i>	39
7.3.3	<i>Effect of using damping between the hammerhead and the impact surface</i>	40
7.3.4	<i>Effect of using clay damping on the fixture</i>	41
7.3.5	<i>Effect of changing the weight of the mockup</i>	42
7.3.6	<i>Effect of changing the distance from the impact to the test item</i>	43
<b>8.</b>	<b>A COMPARISON WITH A DROP TABLE TEST</b>	<b>46</b>
<b>9.</b>	<b>ANALYSIS OF THE FIXTURE</b>	<b>47</b>
9.1	MOBILITY MEASUREMENT	47
9.2	FEM ANALYSIS OF THE FIXTURE	49
9.3	THE FIXTURE'S MODE SHAPES	49
<b>10.</b>	<b>CONCLUSIONS OF THE FIXTURE ANALYSIS</b>	<b>51</b>
<b>11.</b>	<b>ANALYSIS OF TEST ITEM</b>	<b>52</b>
11.1	THEORY USED BY ANSYS	52
11.2	PROBLEM DESCRIPTION	52
11.2.1	<i>Material data</i>	53
11.3	AVAILABLE METHODS	53
11.3.1	<i>Spectrum analysis</i>	54
11.4	SOLID OR PLATE THEORY MODEL	55
11.5	MAINSTEPS IN THE ANALYSIS	55
11.5.1	<i>Combination of modes</i>	55
11.6	CONCLUSION OF MOCKUP TEST ANALYSIS	56
<b>12.</b>	<b>CONCLUSIONS</b>	<b>57</b>
12.1	CONCLUSIONS	57
12.2	FURTHER WORK	57
<b>13.</b>	<b>REFERENCES</b>	<b>58</b>
	<b>Appendix A</b>	<b>60</b>
	<b>Appendix B</b>	<b>64</b>
	<b>Appendix C</b>	<b>71</b>
	<b>Appendix D</b>	<b>73</b>

## **1. INTRODUCTION**

In order to meet new requirements of pyroshock testing a study of techniques for quantifying pyrotechnic shock, pyroshock machines, pyroshock measurements and analysis methods of pyrotechnic shock was done.

Pyroshock, also called pyrotechnic shock, is the response of a structure to high frequency, high –magnitude stress waves that propagate through-out the structure as a result of an explosive event such as the explosive charge to separate two stages of a multistage rocket.

Testing and analysing is strongly connected in investigations about pyrotechnic shock, for example finite element method (FEM) and statistical energy analysis (SEA) require inputs such as damping or coupling loss factors. These factors are empirical and must be obtained by measurements of shock.

In our case the specification is presented as a shock response spectrum (SRS). A discussion about SRS and its advantages, is given further on.

The characteristics of the pyroshock acceleration time-history vary with the distance from the pyroshock event. In the near field, which is very close to the explosive event, the pyroshock acceleration time-history is a high-frequency, high amplitude shock that may have a transient part with a duration of microseconds or less. In the far field, which is far enough from the event to allow structural response to develop the acceleration time-history of the pyroshock approximates a combination of decayed sinusoids with one or more frequencies.

## **2. HOW PYROTECHNIC SHOCK CAN AFFECT ELECTRONIC COMPONENTS**

Pyrotechnic shock techniques have been proven to be very effective for performing functions such as stage separation on missiles and opening large doors on spacecraft. Pyrotechnic techniques are reliable, lightweight, and low-cost. They are used extensively by airframe companies to perform a wide variety of complex task, replacing larger and heavier hydraulic pumps, electric motors, solenoids, linkages, and actuators. Pyrotechnic events, however, often generate high acceleration levels and high exciting frequencies. Extra care must be used to ensure the structural integrity of the various structural members, such as housing, circuit boards, electronic components, interconnect boards, cables and harnesses, that may be affected by the high-level shock. Certain types of electronic components are sensitive to high-level pyrotechnic shock. Components with large, flat, thin sheet metal covers, typically found on hybrids and pin grid arrays, may experience large displacement in these covers. When there are insufficient internal clearances, this may cause internal short circuits. These failures are difficult to trace, since the components suffer no adverse effect and they still work after the shock exposure [1].

### 3. PYROSHOCK TESTING

#### 3.1 Standard Shock-testing machines

##### 3.1.1 Shock machines

Shock machines such as the drop tables (see figure 1) are not suitable for pyroshock simulation. These machines provide to the test item a kinetic energy that is converted into deformation energy when the shock occurs meanwhile pyrotechnic devices generally produce little or no net velocity change. The single-sided pulses produced by these machines bear little or no resemblance to the pyroshock acceleration transient; such pulses produce significantly greater velocity change than a pyroshock environment. Strong motivations are their common availability and their low test cost.

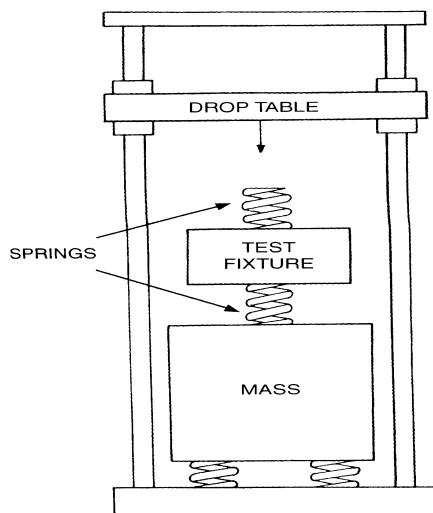


*Figure 1: Drop table.*

##### 3.1.2 Electrodynamic Shakers

Pyroshock environments can be simulated with an acceleration transient produced on an electrodynamic shaker. In this method the acceleration transient is synthesised so that its shock spectrum will closely match the test requirement. With this method a relatively complex shock spectrum shape can be matched within close tolerance up to about 3000 Hz and amplitude of 300 G's. Some shakers have [2] a special construction allowing them to reach 9000 G's [3]. They are sometimes used but care has to be taken in order that they not generate a time-history that looks like a vibration instead of a pyroshock. Such systems tend to act on the dynamic amplifications factor in order to get high amplitudes in SRS while maintaining low amplitude time domain excitation. These electrodynamic shakers are unable to provide sufficient excitation above 5 kHz.

### 3.1.3 Resonant Fixtures

#### 3.1.3.1 General-Purpose Resonant Fixtures

A variety of resonant fixtures technique have been used to simulate pyroshock environments. All of these methods utilise a fixture or structure which is excited into resonance by a mechanical impact from a projectile, a pendulum hammer, a pneumatic piston, or some how subjected to the resonant response which simulates the desired pyroshock.

When a fixture is excited into resonance by a mechanical impact, its response can provide an adequate pyroshock simulation to an attached test item. The response of the fixture is dependent on a large number of parameters including:

- the geometry and the materials of the fixture
- impact mass or speed
- impact duration which is controlled with various impact materials
- impact locations
- test item location
- various clamp and suspension mechanisms

#### 3.1.3.2 Full-Scale Tests.

Some mechanically excited simulation techniques involve the use of an actual or closely simulated structure (e.g., an entire missile payload section). The pyrotechnic devices (e.g., explosive bolt cutters) normally located on this structure would then be replaced with hardware that allows a controlled impact at the same location. Since a closely simulated structure is used, it is anticipated that the impact will cause the modes of vibration of the structure to be excited in a manner similar to the actual pyrotechnic source. In principle, test amplitudes can be adjusted by changing the impact speed or mass. This method is relative expensive due to the cost of the test structure and because significant trial and error is required to obtain the desired test specifications.

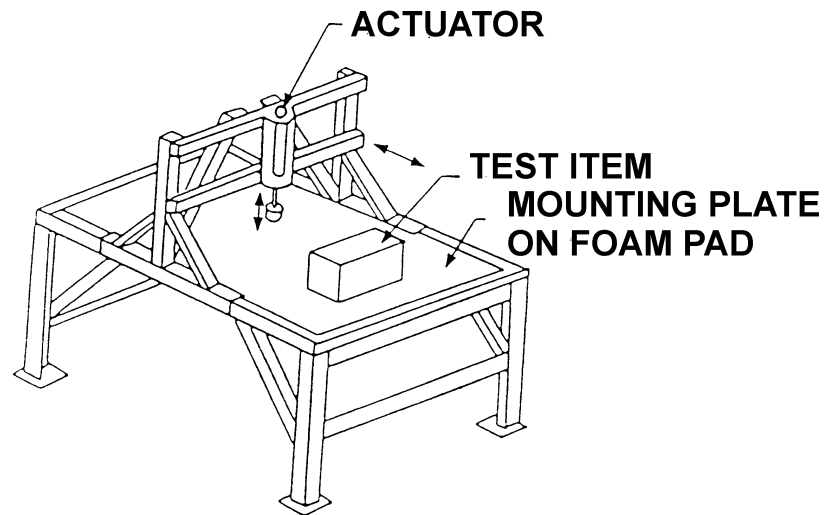
#### 3.1.3.3 MIPS (Mechanical Impulse Pyro Shock) Simulator:

The MIPS simulator is a well-developed embodiment of trial- and- error resonant fixture methods. It was developed at Lockheed [4].

Its design facilitates the easy variation of many of the parameters described above. The MIPS simulator consists of an aluminium plate, which rest on a thick pad. The shock is generated by a pneumatic actuator which is rigidly attached to a moveable bridge, facilitating various impact materials (lead, aluminium, steel, etc.) can be used to achieve a variation of input duration.

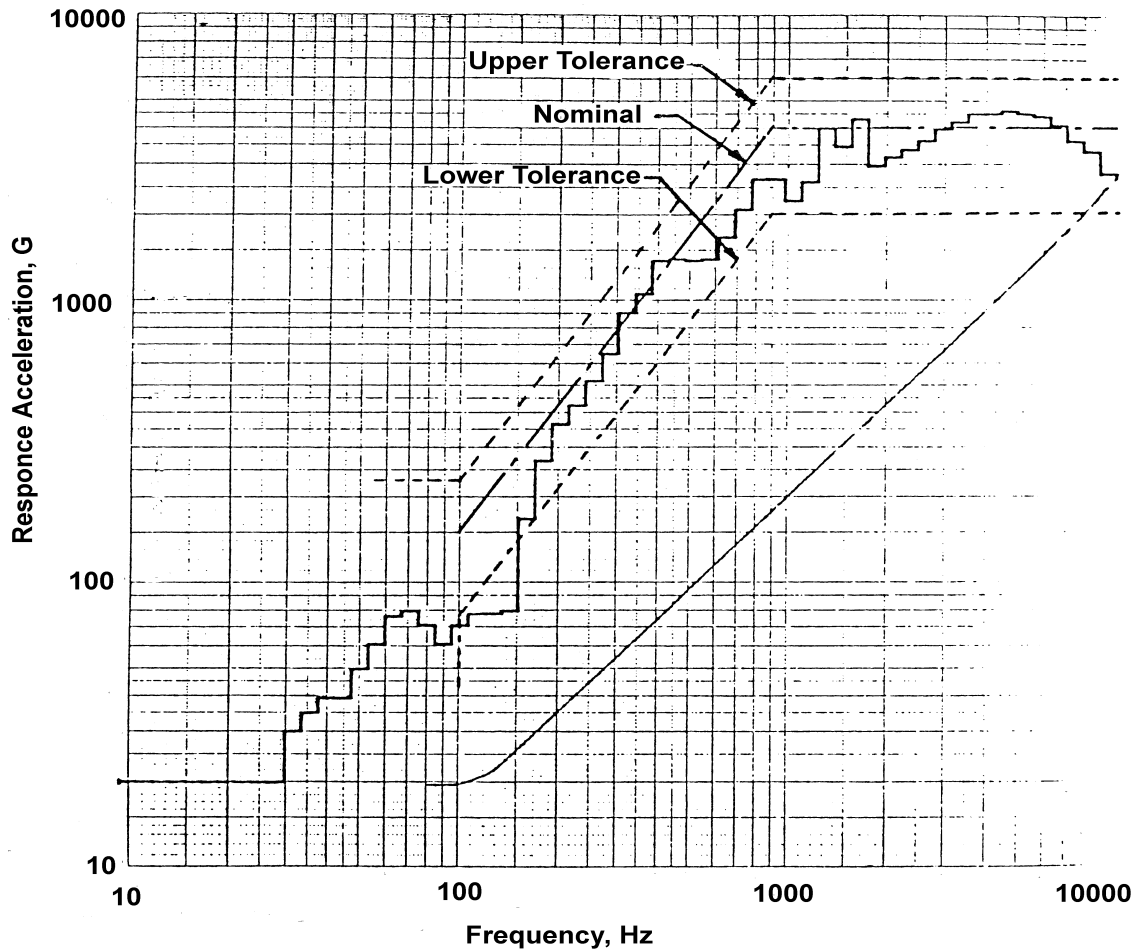
The vertical impact in this case is perpendicular to the plate. Tolerance is also more reasonable for this response spectrum. It is a 4,200-g peak response.

Figure 2 shows a sketch of a general test arrangement. The specimen would be mounted on the plate, and a pneumatic actuator impacts the plate. It is an aluminium plate about 12,5 mm thick and its size is 1,22 m by 1,82 m. The plate has 75 mm foam pad underneath; the rest of the structure and control panel is built up to support the plate and handle it.



**Figure 2:** MIPS simulator. The mounting plate is excited into resonance by an impact from the actuator.

Figure 3 shows response spectra measured using the Lockheed resonance plate system (MIPS). It gives a good idea how well the Lockheed did in meeting the requirements with this particular piece of equipment. The 4200-g spectrum with the tolerance is shown, and they met it pretty well except at low frequency.



Distance – Unit to measurement	= 62 mm (2,5 inch)
Distances – Measurement to Impact Point	= 162 mm (6,5 inch)
Actuator Pressure	= 150 psi
Damping	= 15 sheets paper

**Figure 3:** Response Spectra Measured on the Lockheed Resonant Plate System, Initial Conditions

#### 3.1.3.4 Changing the characteristic of SRS for the MIPS simulator

The MIPS simulator was used to determine how different characteristic of the test setup affect the response spectrum. The change parameters are: actuator pressures, the damping, the impact distance of and added felt pad [4]. The effect on the response spectra are shown in the following figures.

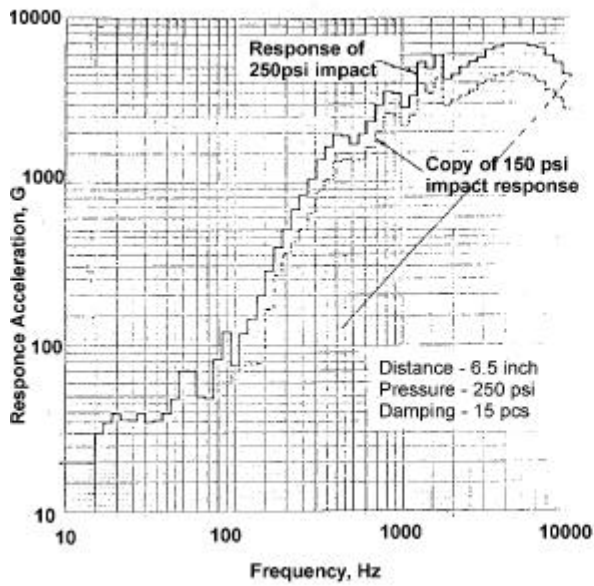


**Figure 4:** Effect of change in Actuator pressure on response of the Lockheed Response Plate System.

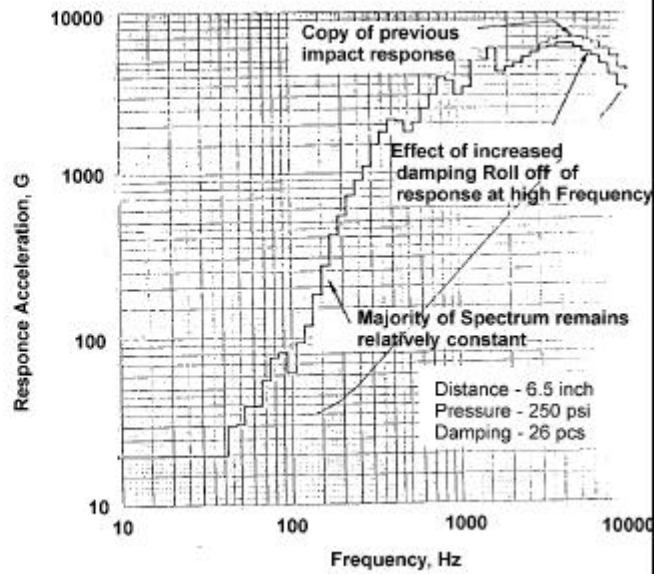


**Figure 5:** Effect of change in damping.

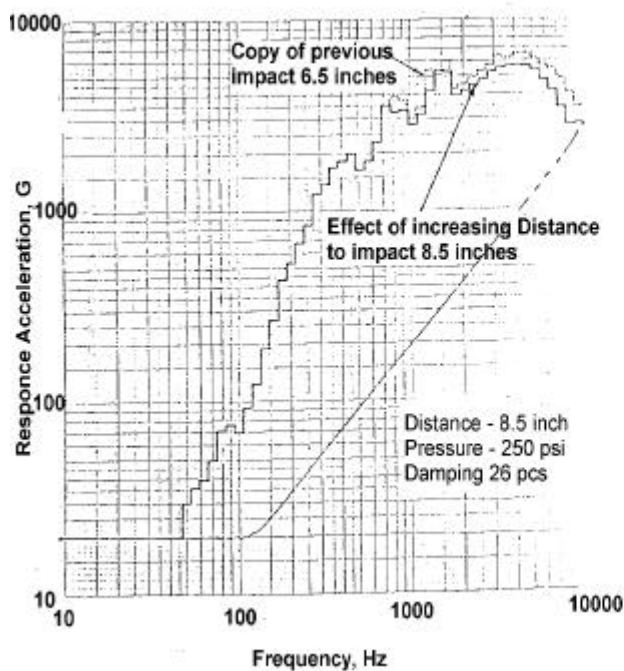


**Figure 6:** Effect of change in distance from Impact point.

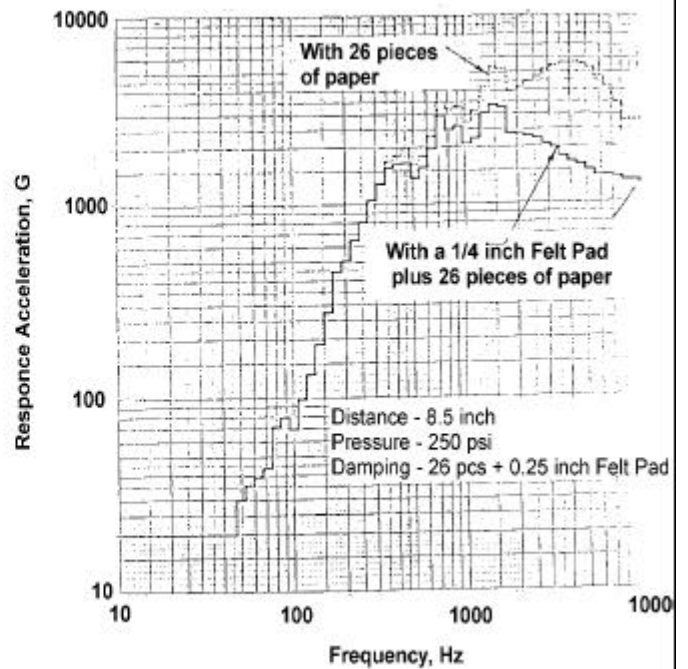


**Figure 7:** Effect of addition of Felt Pad.

### 3.1.4 Tuned resonant fixtures

It is possible to greatly reduce the amount of trial- and error- required by MIPS Simulator and other resonant fixture methods. In order to do this; a simple resonant fixture is analytically designed so that its dominant response frequency corresponds to the dominant frequency in the shock spectrum test requirement. These tuned resonant fixtures are primarily limited to pyroshock environments that exhibit more or less typical characteristics with knee frequencies up to 3000 Hz [2]. The basic design principle is to match the dominant fixture response, with the shock spectrum knee frequency. When this fixture is excited into resonance, it will have the desired shock spectrum knee frequency and the typical 9 dB/octave initial slope.

Relative thick and massive resonant fixtures are required in comparison to the structures to which the test item might be attached in actual use. One significant advantage of using a thick resonant fixture is that its not greatly influenced by the attached test item. This allows the same test apparatus to be used for a variety of different test items.

When using tuned resonant fixtures, the test item is usually attached to an intermediate fixture such as a rectangular aluminium plate. This adapter fixture must be small enough and stiff enough so that the input from the resonant fixture is not significantly altered. Since the resonant fixture is designed to produce the pyroshock simulation in only one direction, the adapter fixture should be designed so that it may be rigidly attached to the resonant fixture in three orientations (e.g., flat down, and on each of two edges). The acceleration input should be measured next to the test item on the adapter fixture.

A number of different techniques are used to provide the mechanical impact required by the tuned resonant fixture methods described below. Pendulum hammers have been used, as well as pneumatically driven pistons or air guns. Whatever method is selected, it must allow repeatability, and control of the impact force magnitude and duration. The magnitude of the impact force will control the overall test amplitude, and the impact duration must be appropriate to excite the desired mode. Placing various materials (e.g., felt, cardboard, rubber, etc.) on impact surfaces usually controls the magnitude of the impact force.

#### 3.1.4.1 Resonant Plate (Bending Response)

The resonant plate test method is illustrated in figure 8 which shows a plate freely suspended by some means such as bungee cords or ropes. A test item is attached near the centre of one face of the plate that is excited into resonance by a mechanical impact directed perpendicular to the centre of the opposite face. The resonant plate is designed so that its first bending mode corresponds to the knee frequency of the requirement. The plate must be large enough so that the test item does not extend beyond the middle third of the plate.

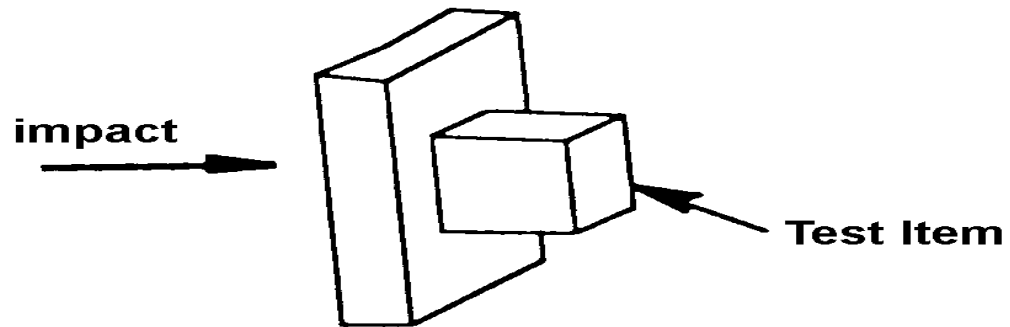


**Figure 8:** Resonant Plate Test method.

### 3.1.4.2 Resonant Bar (Longitudinal Response)

The resonant bar concept is illustrated in figure 8, which shows a freely suspended bar with a rectangular cross-section. A test item is attached at one end of the bar, which is excited into a resonance by a mechanical impact at the opposite end. The basic principle of the resonant bar test is exactly the same as for a resonant plate test except that the first longitudinal mode of the bar is utilised. The bar length required for a particular test can be calculated with the equation below [2].

$$L=c/2f$$

Where:

L= bar length

c= wave speed in bar

f= knee frequency (Hz)= first longitudinal mode.

The other dimensions of the bar can be dimensioned to accommodate the test item, but they must be significantly less than the bar length. As with the resonant plate method the response of the bar can be damped with clamps if needed. These are most effective if attached at the impact end.

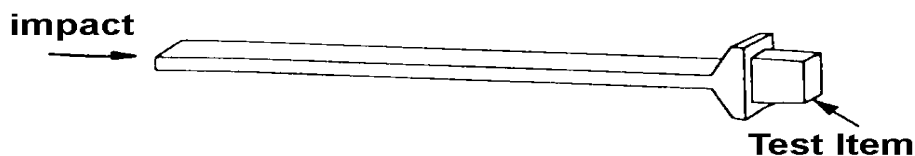


**Figure 8:** Resonant Bar Test Method. The first longitudinal bar mode is excited by an impact as shown. The bar's response simulates far-field pyroshock for the attached test item. The bar is sized so that its first longitudinal mode corresponds to the desired knee frequency of the test.

### 3.1.5 Tunable Resonant Fixtures with an Adjustable Knee Frequency

The tuned resonant fixture methods described previously can produce typical pyroshock simulations with knee frequencies that are fixed for each resonant fixture. A separate fixture must be designed and fabricated for each test requirement with a different knee frequency, so that a potentially large inventory of resonant fixtures would be necessary to cover a variety of test requirements. For this reason tunable resonant fixture test methods were developed which allow an adjustable knee frequency for a single test apparatus.

#### 3.1.5.1 Tunable Resonant Bars

The frequency of the first longitudinal mode of vibration of the resonant bar shown in figure 9 can be tuned by attaching weights at selected locations along the length of the bar. If weights are attached at each of the two nodes for the second mode of vibration of the bar, then the bar's response will be dominated by the second mode ( $2f$ ). Similarly, if weights are attached at each of the three nodes for third mode of bar, then the third mode ( $3f$ ) will dominate. It is difficult to produce this effect for the fourth and higher modes of the bar since the distance between nodes is small to accommodate the weights. This technique allows a single bar to be used to produce pyroshock simulations with one of three different knee frequencies.

#### 3.1.5.2 Tunable Resonant Beams

Figure 10, illustrates a tunable resonant beam apparatus, which will produce typical pyroshock simulations with a knee frequency that is adjustable over a wide frequency range. In this test method, an aluminium beam with a rectangular cross section is clamped to a massive base as shown. The clamps are intended to impose nearly fixed-end conditions on the beam. When the beam is struck with a cylindrical mass fired from the air gun beneath the beam, it will resonate at its first bending frequency, which is a function of the distance between the clamps.

This method provides a good general-purpose pyroshock simulator, since the knee frequency is continuously adjustable over a wide frequency range (e.g., 500 to 3000 Hz).

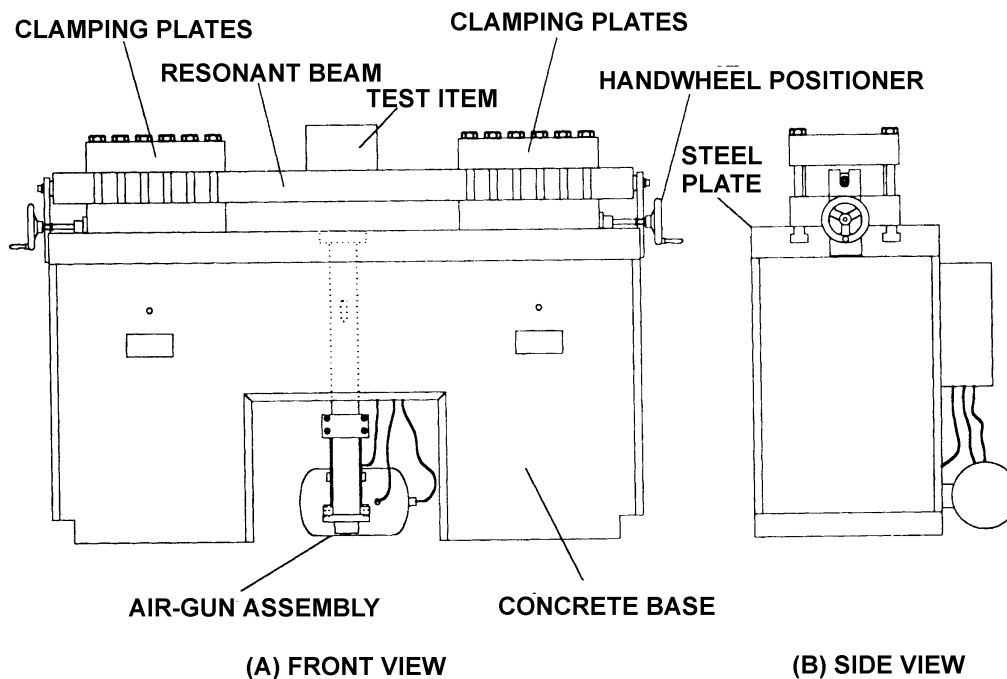


**Figure 10:** MIPS simulator. The mounting plate is excited into resonance by an impact from the actuator. The plate response simulates far-field pyroshock for the attached test item.

## 3.2 Measurement techniques

Measurement of pyroshocks are generally made with accelerometers, strain gages or laser Doppler vibrometers (LDV). The accelerometers are used to measure acceleration, and strain gages and LDV are used to measure velocity. The strain gages may also be used to sense force, stress or strain.

### 3.2.1 Accelerometers

Accelerometers are widely used for the measurements of pyroshocks, primarily because of their convenience, even though they can introduce serious problems when used for near-field pyroshock measurements. However, there are other types of transducers that might be used in place of accelerometers for near-field measurements.

Care must be taken to protect accelerometers from resonance and, in some cases, failure. If accelerometers are excited at resonance, large amplitude outputs result and may exceed the maximum amplitude of the data acquisition system that was chosen for the test. The result is that the data magnitudes are clipped. If the data are clipped, it is rendered useless, and the results from the test will be greatly diminished.

### 3.2.2 Strain gages

Strain gages can be used to measure intense, near-field pyroshocks with few problems, and are recommended when the actual surface strain in a structure is of interest. However, surface strain measurements on a structure are difficult to translate into the orthogonal motions needed to arrive at design and test criteria for equipment mounted on that structure.

### 3.2.3 Laser Doppler vibrometer (LDV)

The LDV is a non-contact system that measures the Doppler shift of a laser beam reflected from a target on the moving or vibrating surface. The system must have a fixed or non-moving reference, which generally restricts it to the laboratory test, where a fixed foundation can be obtained.

LDV constitutes an attractive alternative to accelerometers for laboratory pyroshock measurements in that they [2]:

- Directly measure motion.
- Make no physical contact with the structure.
- Have no resonance problems.
- Easy to set up.

The LDV has the following disadvantages:

- Very expensive per channel in comparison to the other measurements techniques.
- Difficult to calibrate.
- You must have line sight to the measurement location.
- Lower dynamic range compared to an accelerometer.

Laser vibrometers have been successfully used to measure pyroshocks within 25 mm of the source, where the shock magnitude exceeds 80 000 g [5].

## 3.3 Loading

Two pyroshock simulation techniques exist:

- Mechanically excited simulations.
- Pyrotechnically excited simulations.

A short duration mechanical impact on a structure causes a response similar to that produced by a pyrotechnic source. These mechanically excited simulations cannot produce the very high frequencies found in near-field pyroshock. Mechanically excited simulations allow control of dominant frequencies up to about 10 000 Hz.

A far-field pyroshock requires frequency control no higher than 10 kHz; a mechanically excited simulation technique is thus appropriate. The far field contains not only lower frequency, but also lower g-levels than near-field pyroshock. Most of the energy is usually concentrated at one or at a few frequencies, which correspond to dominant structural mode(s).

A near field pyroshock test requires frequency control up to and above 10 000 Hz. A pyrotechnically excited simulation technique is appropriate.

### 3.3.1 Mechanical impacts

For mechanical impact, the main parameters affecting the shock amplitude, shape and the direction are the type of [6]:

- Test fixture.
- The impact direction.
- The distance from impact point to test item.
- The anvil material.
- Hitting tip material.
- The dropping mass weight.
- The dropping height (missile speed if air gun is used).

Comparison of some of these parameters are discussing in the *measurement chapter 7*.

#### 3.3.1.1 Effect of the type of excitations

The dropping mass excitation gives more amplitude at low frequency than the air gun does [6].

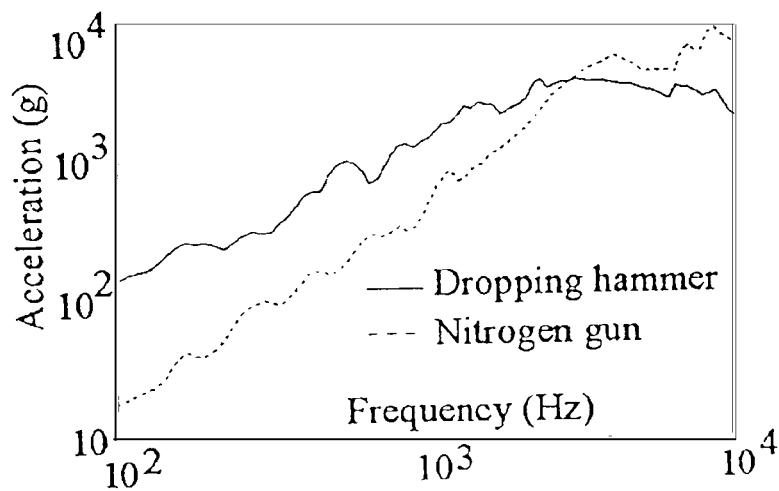


*Figure 11: Dropping mass or Air Gun excitations.*

### 3.3.1.2 Effect of impact head materials

Different impact materials give different impact duration. A comparison is made between two shocks obtained with an impact head made of steel and an impact made of brass (see figure 12). This parameter affects the SRS shape.

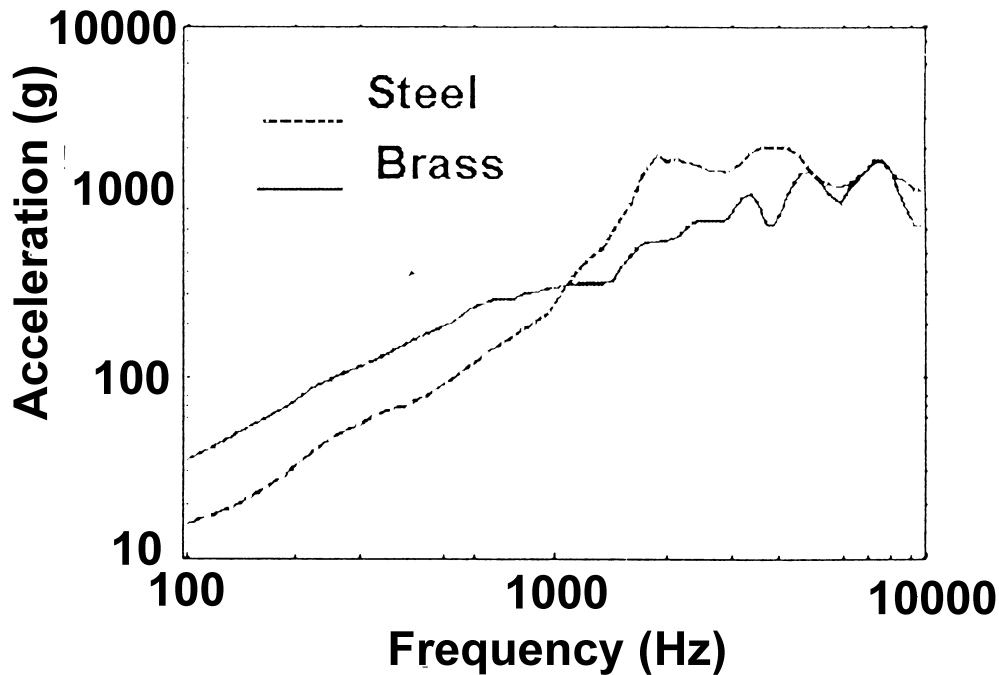


*Figure 12: Effect of impact head material.*

### 3.3.2 Pyrotechnically impacts

The test item is mounted to one side of the fixture. The explosive charge is usually attached to the backside or edges of the test fixture (contact explosion). It can also be mounted on a second test fixture not in direct contact with the primary test fixture (non contact explosion) [6].

The advantages of this technique are:

- Its ability to achieve high frequencies and to generate transient excitation along all axes at the same time [2].
- When such a system is well in hand of the test staff, it can produce pyroshock simulations that match the requirements in all directions.

The disadvantages are:

- Numerical simulations is very difficult .
- The decreasing of the amplitude at high frequency is difficult.
- The ordance test generates dust.
- A qualified explosives facility (with its associated safety procedures) is required.

A good choice of detonators [6] is NONEL. This generates less electromagnetic pulse than electrical detonators. This is especially important when operating electronic units are tested.

The magnitude and shape of the resulting pyroshock are controlled by:

- Test fixture (type and material).
- Contact or non-contact explosion.
- Location and the size of the explosive charge.
- Explosive charge mounting details.
- Locations of the test item on the test fixture.

For more information about measurement result and SRS curves see reference [6].

### **3.4 Measurements problems**

#### **3.4.1 Accelerometer problems**

- Accelerometers must be chosen and mounted carefully. Use only accelerometers designed for shock testing. These accelerometers should be selected to have a first natural frequency and a maximum g level well above those required for the shock. However, high g level accelerometers have low sensitivities, resulting in relatively high-noise floors. Thus the engineer must balance high g capabilities with instrumentation noise.
- Accelerometers must be mounted according to manufactures' specifications to ensure that the accelerometer performance will meet the published specifications. Shock accelerometers should be mounted with a stud, or with two short screws. All mounting must be on flat, clean surfaces with good surface finishes.

#### **3.4.2 Mass-loading effect**

Will the weight variations in mounted subassemblies affect the shock environment of the system? This effect is the, so called, Mass-loading effect. It is clear that the mounted equipment will have some effect on the load environment, but is the effect so big it should be considered in the model?

A laboratory test to simulate pyroshock shows that if the subassemblies mass is small, it will not affect the shock environmental much [21]. The SRS assumes no mass loading effect. Mass-loading effect decreases if a low weight accelerometers is used.

## 4. TECHNIQUE FOR QUANTIFYING PYROSHOCK

### 4.1 The shock response spectrum model (SRS)

Shock pulses can be very simple or very complex. When they have simple shapes such as square, sine, or triangular, they are easy to describe and understand [9]. Pulse shocks are easy to work with because the mathematics is simple and convenient. Various types of simple shock pulses are shown in figure 13.

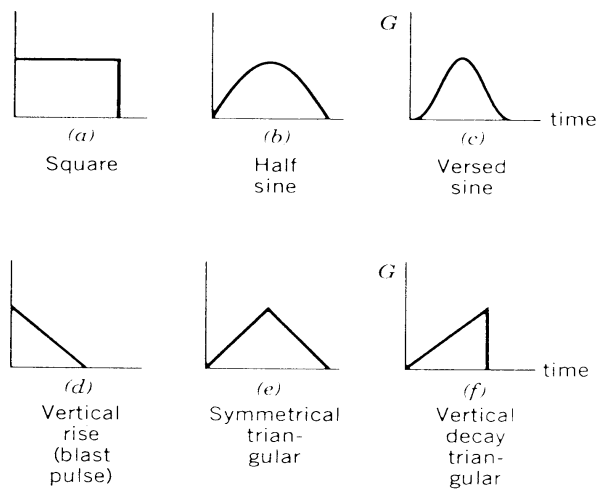


**Figure 13:** Various types of simple shock pulses.

However, when shock pulses are complex, it is easier to describe how a structure responds to the shock rather than try to describe the shock motion itself. For this purpose the shock response spectrum (SRS) is appropriate, as it shows the damage potential.

The shock spectrum is widely used to analyse pyroshock data and provides a measure of the effect of the pyroshock on a simple mechanical model. SRS applies an acceleration time history as a base excitation to an array of single degree of freedom (SDOF) systems (see figure 14). For explanation of SRS see Appendix A.

Generally, a measured acceleration-time history is applied to a single degree of freedom model, and the maximum acceleration response is calculated. An ensemble of maximum absolute value acceleration responses is calculated for various natural frequencies of the model. A curve representing the responses as a function of the damped natural frequency is called a shock spectrum and is normally plotted with log-log scales.

Velocity shock spectrum and displacement shock spectrum may be calculated, but are not commonly used for pyroshock specification [7]. See Appendix A for an explanation and an example of the SRS.

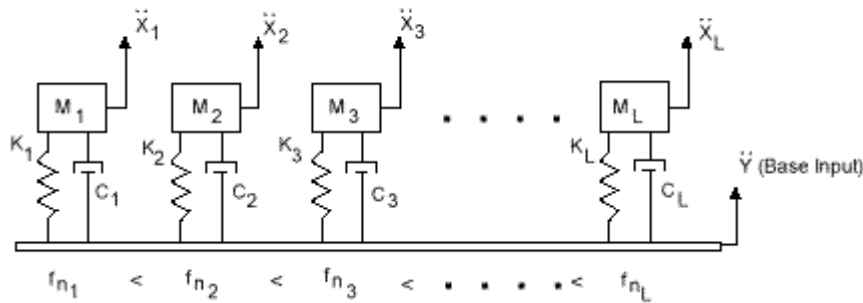


**Figure 14:** Shock Response Spectrum Model

Note that each system *is not assumed* to have a, so called, *mass-loading* effect on the base input. see headline Mass-loading effects.

- ..
- Y is the common base input for each system, and the double-dot denotes .. acceleration
- $X_i$  is the absolute response of each system to the input.
- $M_i$  is the mass
- $C_i$  is the damping coefficient
- $K_i$  is the stiffness for each system
- $F_{ni}$  is the natural frequency for each system.

#### 4.1.1 Damping

A typical value of the damping ( $\zeta$ ) is 5%, which is equivalent to  $Q = 10$ . The damping is a constant without unit:  $\mathbf{z} = \mathbf{C}/2 * \mathbf{\ddot{O}}(\mathbf{K} * \mathbf{M})$ .

- If  $\zeta < 1$ , weak damping.
- If  $\zeta > 1$ , strong damping.
- If  $\zeta = 1$ , so called critical damping.

$Q = 1/C * \sqrt{K * M}$  and thus  $= 1/2 * \zeta$ .  $Q$  is a measure of the system damping, and is normally called the *quality factor* of the system and the larger value of  $Q$  the smaller is the damping [18]. For a completely undamped system  $Q$  approaches infinity. While for a critically damped system  $Q = 1/2$ . An approximate measure of  $Q$  is obtained in practise by measuring the width of the response curve  $|H(\omega)|$ . The damping of the model is held constant at a value such as 5% for various natural frequencies. (5% is the most commonly used value).

Any set of unique natural frequency of the model can be used for the spectrum calculation. A typical scheme however, is based on a proportional bandwidth, such as a 1/6 octave. When proportional bandwidth is used, the response is calculated with larger and larger step length as the frequency increases. The 1/6 Octave bandwidth is almost to consider as a standard in pyroshock world [7].

#### 4.1.2 1/6 Octave bandwidth

The name alludes that each successive natural frequency is  $2^{1/6}$  times the previous natural frequency. A sample set of N calculation frequencies [Hz] would be: 10 11.2 12.6 14.1 ....  $10 \cdot 2^{1/6(N-1)}$ . This means that the bandwidth increases with frequency. The upper ( $f_u$ ) and lower ( $f_l$ ) frequency related to every band can be easily calculated from the formulas:

$$f_l = f_c / 2^{1/12} \text{ and } f_u = f_c \cdot 2^{1/12} \text{ where } f_c \text{ is the centre frequency.}$$

#### 4.1.3 To plot the Shock Response Spectrum

The result of the calculation method is represented in terms of the natural frequency domain and is presented on a log-log scale. The shock spectrum for pyroshock has a characteristically steep slope at low frequencies of 12dB/Octave. That is a direct result of the minimal velocity change occurring in a pyroshock. An example is shown in the figure 15. Typical tolerance bands of  $\pm 6$ dB are drawn about a straight-line approximation of the SRS for testing.

SRS curves are sometimes specified with  $\pm 3$  dB tolerances typical for random vibration testing [7]. These tolerances are too tight for pyrotechnic testing. See Appendix A for explanation about slope and tolerance level.

SRS specifications with relatively high requirements below 100 Hz, can result from data collected with noise in the signal. Real world pyrotechnic SRS levels fall rapidly below 100 Hz. At and above 500 Hz the signal SRS is significantly above the noise SRS. Noise SRS could appear from cable resonance or other non wanted error sources in the measurement equipment. Under 500 Hz the signal could contain too much noise and the SRS will then be useless below 500 Hz.

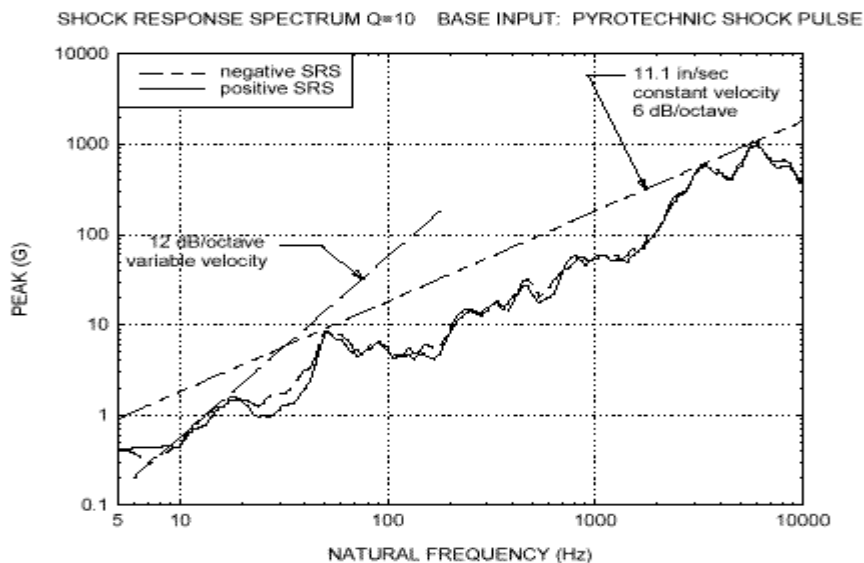


**Figure 15:** A typical SRS curve. Response unit in g ( $9.81m/s^2$ ).

#### 4.1.4 Pyroshock levels

The numerous reflections and recombinations produce pyroshock levels that vary according to the source and the complexity of the carrying structure. They are broadly divided into three categories depending on the distance from the pyroshock generating device [6].

1. *Near-field pyroshocks:*

- Peak acceleration higher or much higher than 5000 g.
- Substantial spectral content above 100 kHz.
- Locations from the source less than 15 cm.

2. *Mid-field pyroshocks:*

- Peak acceleration between 1000 g and 5000 g.
- Substantial spectral content above 10 kHz.
- Locations from the source between 15 cm and 60 cm.

3. *Far-field pyroshocks:*

- Peak acceleration below 1000 g.
- Spectral content below 10 kHz.
- Locations from the source greater than 60 cm.

For a typical far-field pyroshock, the low frequency slope changes at the knee-frequency (see figure 16) and the shock spectrum approaches a constant value at high frequencies that is the peak acceleration in the time domain.

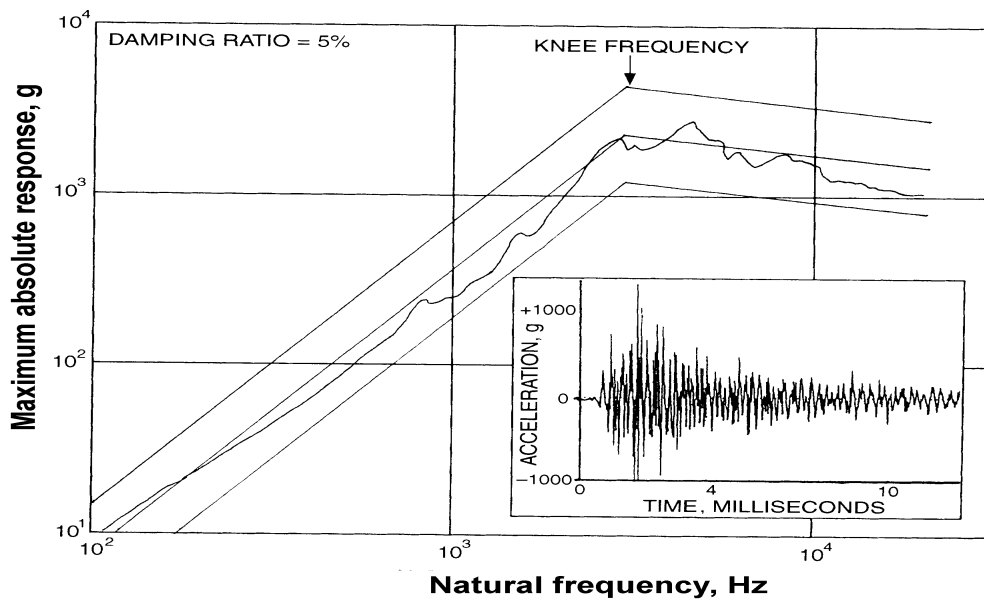


**Figure 16:** Shows a SRS graph with there knee frequency. This graph is calculated from the input (inserted small figure).

#### 4.1.4.1 Advantages and disadvantages of the SRS

One of the main disadvantages of the SRS is that shock environments are often represented using test inputs that are different in character from the original shock. This problem could lead to over conservative tests, especially in the case where simple waveform test inputs are used (such as the sinusoidal signal). Another disadvantage is that the technique is mainly used with linear structures, and linear behaviour. Of course, the techniques are used in connection with failure analysis of structure, but the theoretical development concerned with linear equations.

Since the SRS represents the response of SDOF systems to the measured transient (a transient load has limited duration), it does not yield the peak acceleration that might occur in the response of a multi mode component (a multiple degree of freedom system) subjected to the measured pyroshock. Hence, it is not indicative of the damage potential of the pyroshock to such cases. However, the technique is commonly used and almost to consider as a standard for quantifying pyroshock. There are many reports and programs about SRS available and it provides a conservative test procedure. The simple assumptions made in the SRS (See Appendix A) makes it easier than in other methods, to really understand how the quantifying works.

The SRS is highly sensitive to the assumed damping value for multi-cycle transients like pyroshocks [8].

## 4.2 Alternative methods to quantifying pyroshock

A list and short presentation of some alternative methods is given in this report. For deeper theory of these methods see references.

- The Fourier spectrum
- The Energy spectrum
- Least favourable response (LFR)
- Shock intensity spectrum

### 4.2.1 The Fourier and the Energy spectrum

These provide a description of the transient environment itself rather than the effect of the transient. The energy spectrum is the more applicable of the two methods for the description of stochastic transient, such as pyrotechnic shock, but it has been found lacking in two important ways [2]:

1. The energy spectrum does not define peak accelerations for either the transient or a component subjected to the transient.
2. To achieve statistical stability, the computation of an energy spectrum requires an averaging operation over several repeated shocks, or over frequency in a manner that restricts the resolution of the analysis.

#### 4.2.2 Least favourable response (LFR).

The method of LFR provides a means for defining an upper bound on the response of a linear and non-linear structure excited by a sequence of shock inputs [2]. Advantages of LFR [8]:

1. Generates test input and responses that are conservative (provided that an appropriate measurement point is chosen on the structure).
2. It generates inputs that have the same oscillatory quality as the underlying inputs. Yet, no programs have been found based on the LFR and the technique does not appear to be well developed.

#### 4.2.3 Shock intensity spectrum based on the Fourier energy spectrum

This method is an attractive alternative method to the shock response spectra because it is easy to compute and readily available in many software packages as a FFT (Fast Fourier Transform). A disadvantage with this method is that the phase (The Fourier spectrum is complex) is difficult to interpret and may be contaminated with noise at the high frequencies present in pyroshock [2].

## 5. ANALYSIS METHODS

### 5.1 SEA

Statistical Energy Analysis (SEA) belongs to a category tool used for solving noise and vibration problems that are referred to as “Energy methods”.

These methods look at phenomena of both noise and vibration generation and propagation in terms of energy. The aim is to understand how energy flows in the complex system considered. Variables of interest are derived from the energy variable. In contrast to deterministic methods such as Finite Element Analysis (FEM), SEA are based on a stochastic-or statistical- approach. This means that it is assumed that the dynamic properties of the structure under study can be best described with statistical tools such as mean and variance [22].

### 5.1.1 SEA formulation

The SEA approach is based on a system-level balance. All power flowing into the subsystem must be dissipated within the system or transferred out of the system. This power balance concept is also applied at the subsystem level. A subsystem is defined as a region of resonant modes with the same wave type, and approximately spatially – uniform response in the chosen frequency band. For a structural subsystem, a space-averaged velocity is derived from its energy level as [22]:

$$\langle V^2 \rangle = E/M$$

- $\langle \rangle$  = Space average
- $V$  = Velocity
- $E$  = Stored subsystem energy
- $M$  = Total mass

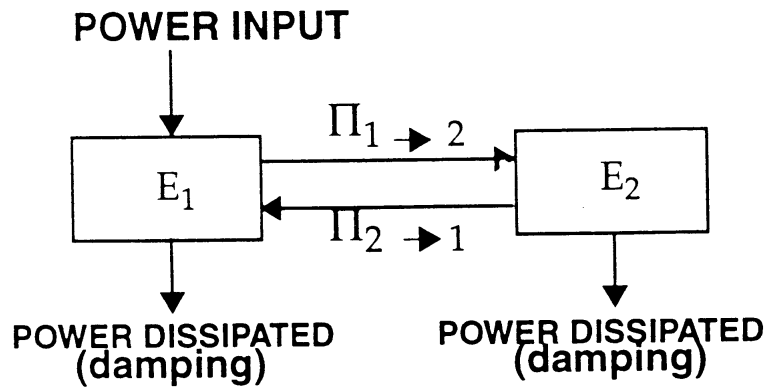


**Figure 17:** Block diagram for a two-subsystem SEA model,  $P_{1 \rightarrow 2}$  is the energy flow from subsystem 1 to subsystem 2.  $E_i$  is the stored energy for subsystem  $i$ .

#### 5.1.1.1 Dissipation Loss Factor (DLF)

The DLF is a measure of how efficient the subsystem can absorb the mechanical power input. The input power, the DLF and the subsystem energy govern the power balance. The larger the DLF, the smaller the subsystem energy for a given power input. In analogy with the DLF, The coupling loss factor (CLF) is a measure of how efficient power can be transmitted between two subsystems [22].

### 5.1.2 Advantages in the use of SEA

SEA has a some advantages [23]:

- Enables analysis at an energy stage in product development, as it utilises a minimal set of input data concerning the system.
- Simplifies the analysis procedure.
- SEA is fast enough to allow major re-design concepts to be tested at any stage of product development.
- Closeness to engineering parameters that governs the flow of energy between subsystems.
- SEA can be used for analysis at high frequency. Few, if any alternative analysis methods can challenge SEA at high frequency.
- Do not demand great deal of computer power.

### 5.1.3 Disadvantages in the use of SEA

SEA has some disadvantages [23]:

- The definition of subsystem is so free that it may become a problem for the SEA analysis.
- The identification procedure of subsystem and transmission paths is manual. The SEA model is always assembled based on the analyst's notion of the system at hand. This feature can make SEA a powerful tool in the hand of the skilled analyst, while it can provide a poor aid in understanding for the first time user.
- Use of the 'geometric' approach in the choice of subsystem for the SEA model can in some cases be dangerous, as the subsystem only represents one type of response coordinate while chosen physical member often contains several types of independent response coordinates (see e.g. below). This leads to more complicated interface towards the user than what's the case with, for example, Finite Element Method. *Example:* Consider a single beam. A full representation of the beam should be represented by four subsystems in the SEA model, contain bending-, longitudinal- and torsional- energies as response coordinates. A graphical representation of the appropriate SEA model does therefore not always look like the system it was made for. It must therefore be recognised that use of SEA relies on the educated user.
- SEA can't handle low frequencies. How low depends on geometry, material etc.
- Correct practise of SEA does in some case lead to prediction of trends rather than absolute levels.
- It's a problem to known in advance in what situations the method should be expected to work and when it may fail.

#### 5.1.4 AUTOSEA2

AutoSEA is a commercial developed computer program based on the SEA principle. In the new version of AutoSEA, called AutoSEA2, the extension module Shock 1.0 will be included. The Shock 1.0 software module predicts highly impulsive shock response including ballistic impact and explosions and pyrotechnic shock response in aerospace vehicles. Separation nuts, gun cutters and explosive cord-separators etc. The software indicates the dominant shock propagation paths and allows design evaluation of attenuation measures including alternative materials, constructions, junction properties and shock isolators.

Shock 1.0 computes an estimate of response in the form of history plots and Shock Response Spectrum (SRS) plots. Shock loads includes rectangular, triangular, half-sine, ramp-exponential, polygonal and user defined loads.

The Shock software will be a very interesting innovation, mostly because the high frequency model for shock response is completed with a deterministic model at low frequencies, but also because it is possible to easily get a SRS as output. In AutoSEA2 it will be possible to import CAD and FE geometry files or interactively create an own geometry.

This program does not, yet exist but a demo version of AutoSea2 is available. Visit the homepage for update information about the demo version:

<http://www.vasci.com/products/shock/index.html>

### 5.2 ANALYTICAL METHODS

Two-degree-of freedom systems could be used to model an electronic box and determine the coupling characteristics of internal modules and PCBs (Printed Circuit Boards) [9]. The outer box or chassis structure is considered to be the first degree of freedom, since this outer structure typically receives the external energy first. After that, the load path goes into the secondary members, such as PCBs, so these members are considered to be the second degree of freedom when the secondary members are fastened directly to outer box structure (see figure 19).

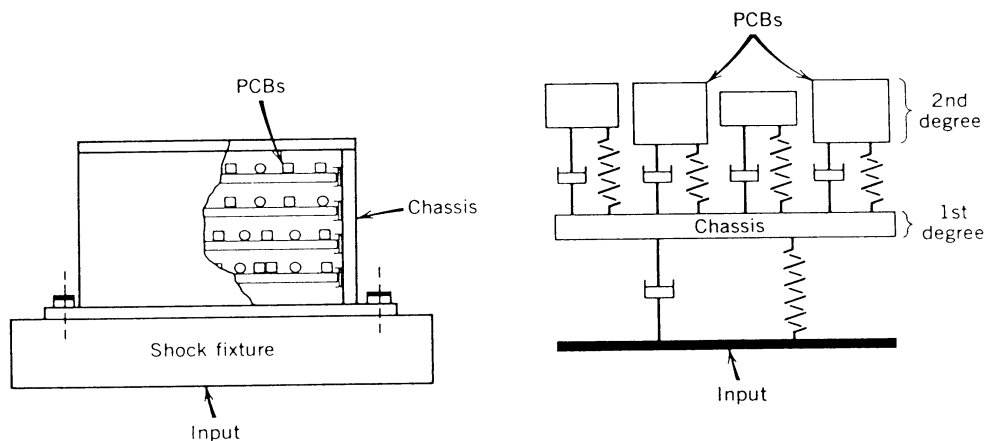


**Figure 18:** Typical representation of chassis and PCB's as two-degree-of freedom system.

When a lightly damped chassis supports lightly damped PCBs it is extremely important to separate the resonant frequencies of the chassis and the various PCBs. When these resonances are not separated by one octave (factor of 2 or more) then the coupling between the chassis and the PCBs can be very severe.

This type of model is of course very general, and doesn't show absolute values for a specific component, but the result could be useful. In many situations the chassis will amplify the shock input and passes it on to the PCBs. The PCB may further amplify the shock they receive, which could result in high PCB accelerations, displacements and stress, leading to possible failures in the components or their solder joints and electrical lead wires.

The shock response for a two-degree of freedom system with light damping is shown in figure 19.

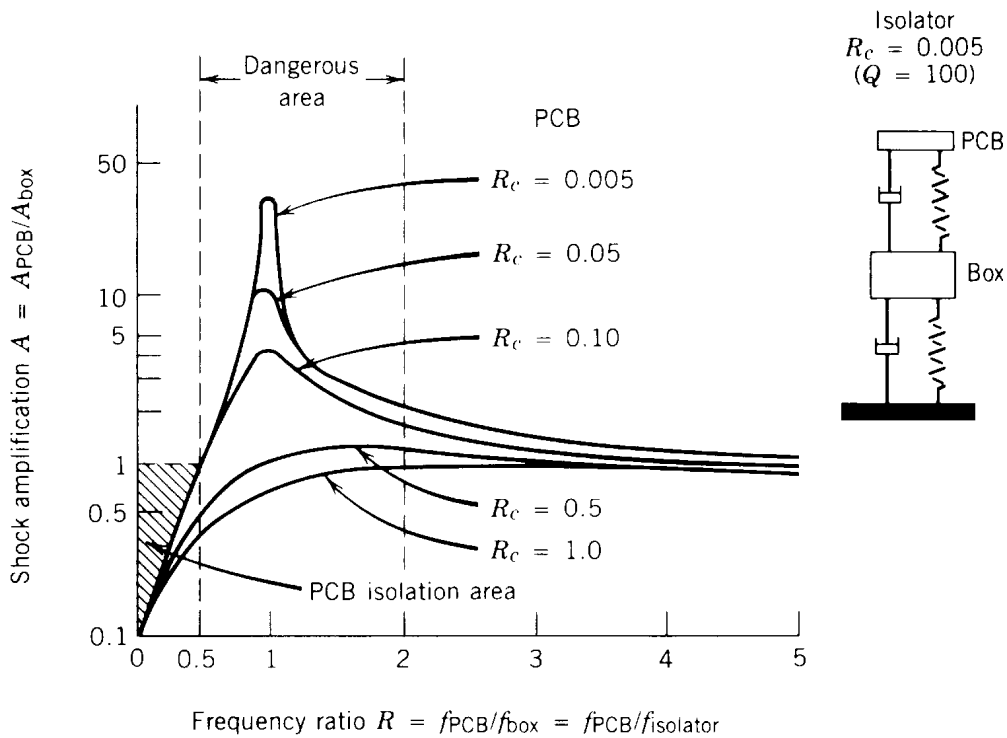


**Figure 19:** Shock response for two-degree-of-freedom system with light damping, showing critical areas that should be avoided ( $R_c = \zeta$ ).

In this system mass 2 (PCB) is small compared to mass 1 (chassis or box). R is frequency ratio between the two natural frequencies of the PCB and the box. Usually the highest shock amplifications will occur in areas that are between the frequency ratios R of 0.5 and 2.0. In this region the shock amplification is only limited by the damping in the system. A lightly damped system will experience higher shock amplifications, and therefore, higher acceleration levels and displacements than the same system with moderate damping.

The shock isolation area (shady) is to the left of the high-amplification region. When the octave rule is followed (see below), the resonant frequency of the PCB will be separated from the resonant frequency of the chassis. Then the coupling effect will be sharply reduced and the effective life of the system will be sharply increased. The magnitude of the shock acceleration levels transmitted to the PCB can be sharply reduced by separating the resonant frequencies of the electronics chassis and the PCBs. It does not matter whether the PCB has a higher resonant frequency than the chassis, or the other way around. As long as their resonant frequencies are well separated, the magnification levels of the PCBs are reduced, so the acceleration levels are reduced. A reasonable amount of separation is about one octave. When the PCB has a resonant frequency that is two or more times the resonant frequency of the PCB, then severe dynamic coupling effects are reduced and the effective life of the system will be increased [9].

### 5.2.1 Advantages and disadvantages

This model could be used in the early design of the circuit boards and chassis, it will give a coarse picture how the response looks like and warn for dangerous design. It is easy to compute when the material parameters are known.

As always the material parameters are difficult to compute and one usually uses measurement techniques. This analytical method fails when it comes to absolute acceleration of a specific component. This is a big disadvantage, it simply means that this method generates general trends instead of absolute values.

## 5.3 FEM

### 5.3.1 Introduction

In practical finite element analysis the procedures are divided into two methods of solution: direct integration and mode superposition.

The two techniques may at first sight appear to be quite different, in fact, they are closely related, and the choice of one method or the other is determined only by their numerical effectiveness.

In direct integration the differential equation  $M\ddot{U} + C\dot{U} + KU = R \dots(1)$  are integrated using a numerical step-by-step procedure.  $M$ ,  $C$  and  $K$  are the mass, damping and stiffness matrices and  $R$  is the vector of externally applied loads.

The term "direct" meaning that prior to the numerical integration, no transformation of the equation into a different form is carried out. In essence, direct numerical integration is based on two ideas. First, instead of trying to satisfy (1) at any time  $t$ , it is aimed to satisfy (1) only at discrete interval  $\Delta t$  apart [10].

The second idea on which a direct integration method is based is that a variation of displacement, velocities, and accelerations within each time interval  $\Delta t$  is assumed.

It is the form of the assumption on the variation of displacements, velocities and accelerations within each time interval that determines the accuracy, stability and cost of the solution procedure. The essence of a mode superposition solution of a dynamic responses that frequently only a small fraction of the total number of the coupled equations need to be considered in order to obtain a good approximate solution to the exact solution of (1). It's primarily because of the fact that in a mode superposition analysis only a few modes may need to be considered. A mode superposition procedure can then be much more effective than direct integration. However, it also follows that the effectiveness must be included in the analysis.

In general, the structure considered and the spatial distribution and frequency content of the loading determine the number of the 10 lowest modes need to be considered. On the other hand for shock loading many more modes generally need to be included. When many time steps need to be included in the analysis the mode superposition may be more efficient than direct integration methods

In Appendix B the difference between implicit and explicit is explained.

### 5.3.2 FEM explicit versus implicit solutions

Implicit methods for time integration suffer from certain drawbacks when compared to explicit schemes, but have also their own advantages. From the user's point of view, the following criteria have to be examined:

- Which method of time integration is better adapted to the type of problem to be solved?
- What is the computer cost of the solution?
- Which method is simpler to use?

The absence of iteration procedures in the solution brings considered simplification in their use, since the only decision that the user has to take in applying the time marching algorithm is to adapt the step length to his/her current problem [13].

Furthermore, practical solutions exist to automatize the choice of the step length, in which case the user may regard an explicit program almost as a black box.

For stability reasons, explicit integration is performed with a very small time step size, but the cost of the large number of time steps is compensated by the very low cost of one explicit step. Therefore, explicit programs are best suited to problems where the high frequency content of the structure contributes significantly to the response, as it could be in the case with transients (high frequency content demands small time step).

Implicit programs, on the other hand, are often characterised by a much higher degree of generality. They benefit from the fact that the time step length is not so strongly limited by stability considerations and that the cost of one time step is thus a not so critical criteria of performance [10].

The recourse to large time step sizes limits the type of problems that can be solved efficiently with an implicit code to transients with frequency content in the lower range. How low depends on the problem.

When applied to linear problems, implicit codes are neither more difficult to apply nor to implement than explicit. This comparison is no longer true when dealing with non-linear problems. Due to the implicit character of the time integration scheme, achieving dynamic equilibrium that is indispensable to control the accuracy of the solution involves elaborate methods of solution for large systems of non-linear equations.

The user is then faced with a broad variety of choices such as:

- Selection of given time integration algorithm.
- Choice of a tolerance in the verifications of dynamic equilibrium.
- Choice of a method for non-linear iterations within a time step or, more generally, of a strategy for non-linear iterations.
- Choice of the time step length, not only according to the physics of the problem, but also to the convergence of the iteration procedure within the time step.

There are thus three ways to reduce the cost of implicit program to non-linear problems:

1. Choosing algorithms that allow for large time step without encountering convergence difficulties.
2. Defining methods and strategies of iteration, which lead to a minimum number of iterations within a time step.

Despite these negative remarks, there are a large number of these codes, mainly by the variety of their finite element library, compared to explicit codes, which may undergo a significant deterioration in their performances when their possibilities are calculated.

### 5.3.3 Mode superposition

For a small number of time steps the direct solution is cheaper, but there will always be a cross over point where the modal solution is cheaper. If more than one load case has to be solved then the modal solution is much more attractive since the eigenvalues only have to be found once. The cost of the step by step solution just accumulates in a linear manner as the number of time steps increases [24].

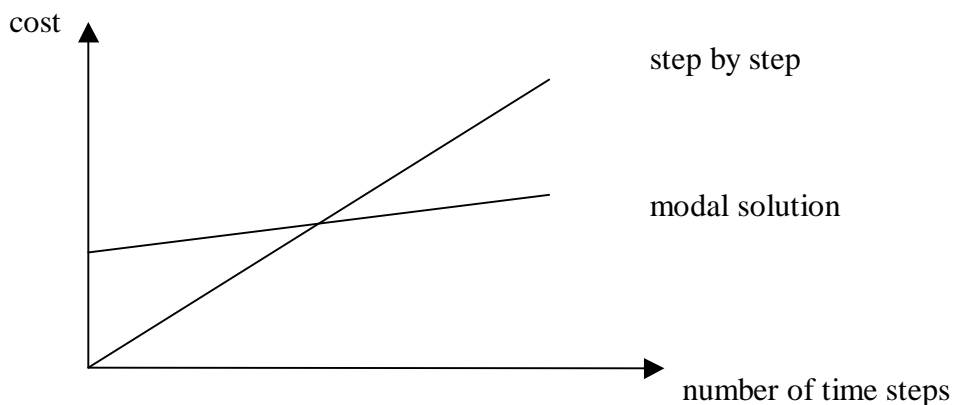


**Figure 21:** Relative solution cost against time of response.

A pyrotechnical analysis demands many time steps because many frequencies have to be included. Many frequencies also means that a great number of time steps have to be included. For this reason the mode superposition method is chosen as analysis method.

## 6. TEST FACILITY DESCRIPTION

### 6.1 Pyroshock test description

#### 6.1.1 Statement of the problem.

In order to meet new requirements of pyroshocks testing a study of pyroshock measurement was done. The aim of the study is to show how to achieve:

- A good repeatability.
- How to change Shock Response Spectrum (SRS) for different requirements.
- According to quality standard (ESA or NASA standard).

#### 6.1.2 Test facility description

A current pyroshock testing apparatus was used to determine how different characteristics of the test setup affect the response spectrum.

The used pyroshock testing machine consists of:

- A stable aluminum frame.
- A freely suspended triangular aluminum plate.
- An impactor, in this case a dropping hammer.

The following methods were used to obtain the:

##### 1. Repeatability:

- By mounting of a protractor a better repeatability was reached. The hammer position was given on the protractor.
- The differences between positive and negative SRS curves should be small.

##### 2. Change of SRS:

- Modify impact hammer. Adjustable weights can be mounted on the hammer head. This causes an easy way to change the SRS.
- Damping material was used to change the the level of the SRS curve.
- Mass damping was used to try to change the knee frequency.

## 6.2 Data Acquisition

### 6.2.1 Test setup

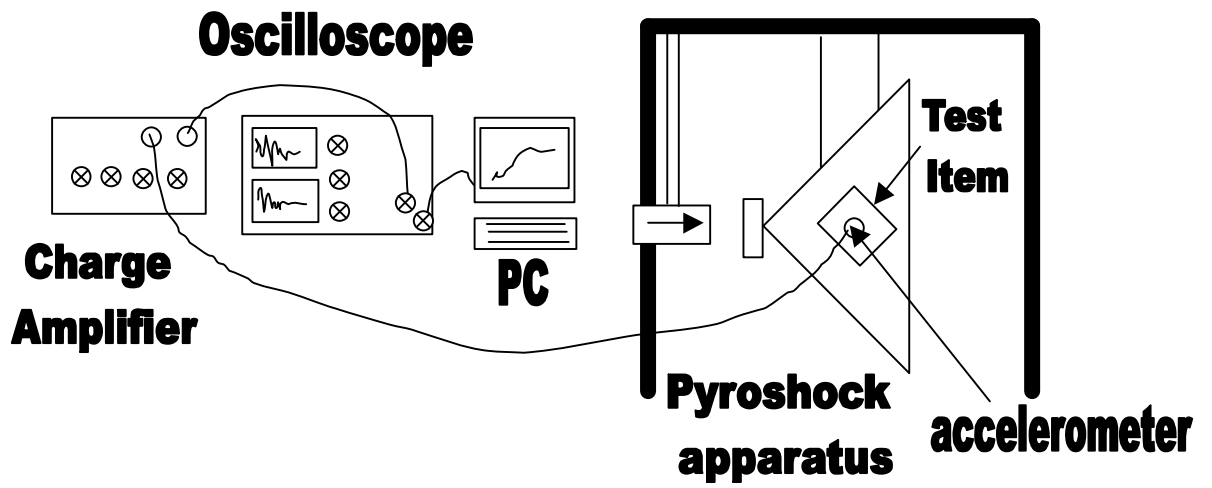


*Figure 23: Test Setup*

### 6.2.2 Test facility description

A spectral analyser is generally used to measure the SRS. In this pilot study an oscilloscope and a PC were used instead. The procedure to do a pyroshock measurement is shown in the figure 24. A users manual, which describes the different step and the program, is attached in the appendix D.

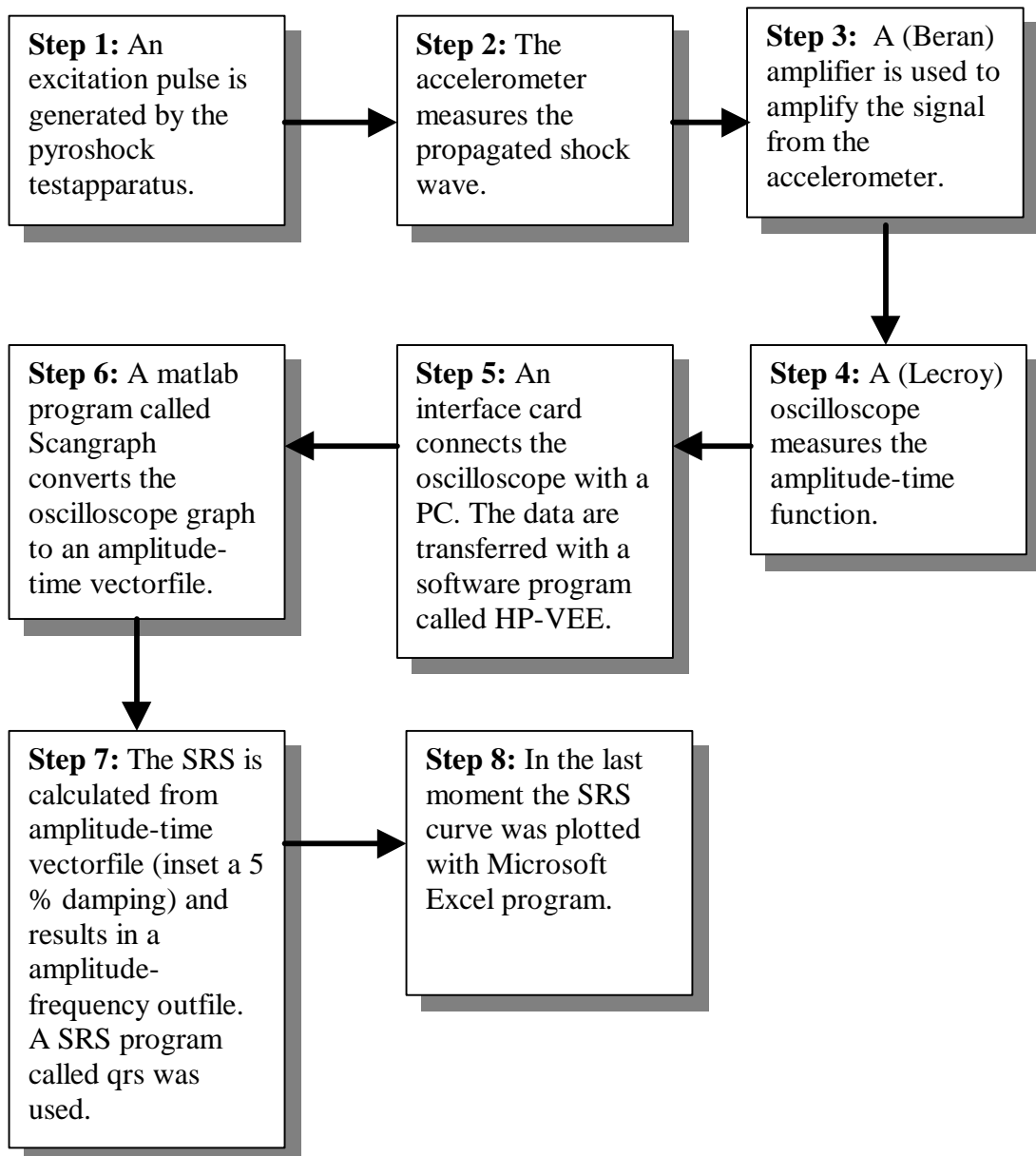


*Figure 24: Pyroshock measurement procedure.*

### 6.2.3 Accelerometers

A piezoelectric accelerometer (ENDEVCO Model 2222C) was used. It's lightweight, 0.5 gm without the low –noise replaceable cable, and effectively minimizes mass loading effects. This type of accelerometer can be exposed for a shock pulse of 10 000 g and is accurate in the frequency range 20 Hz to 10 000 Hz. All our SRS curves have a peak around 40 kHz. This peak is depending on the accelerometers resonant frequency (39.9 kHz).

Four accelerometers of this model were used. In their calibration paper we read that the maximum transverse sensitivity (The accelerometers sensitivity for horizontal vibration) varied from 0.5% (accelerometer 4 in SRS graph) to 2.9% (accelerometer 1 in SRS graph). A lower value gives a higher accuracy. A comparison of the two accelerometers was done. The two accelerometers were mounted beside each other so they get the same vibration into the accelerometers. The result is show in the figure 25.

The differences between the accelerometers are not very large, but the accelerometers with so low transverse sensitivity as possible are preferred. The accelerometers are mounted with glue. The connecting cables are mounted in the opposite direction to the accelerometer with tape to avoid cable noise.

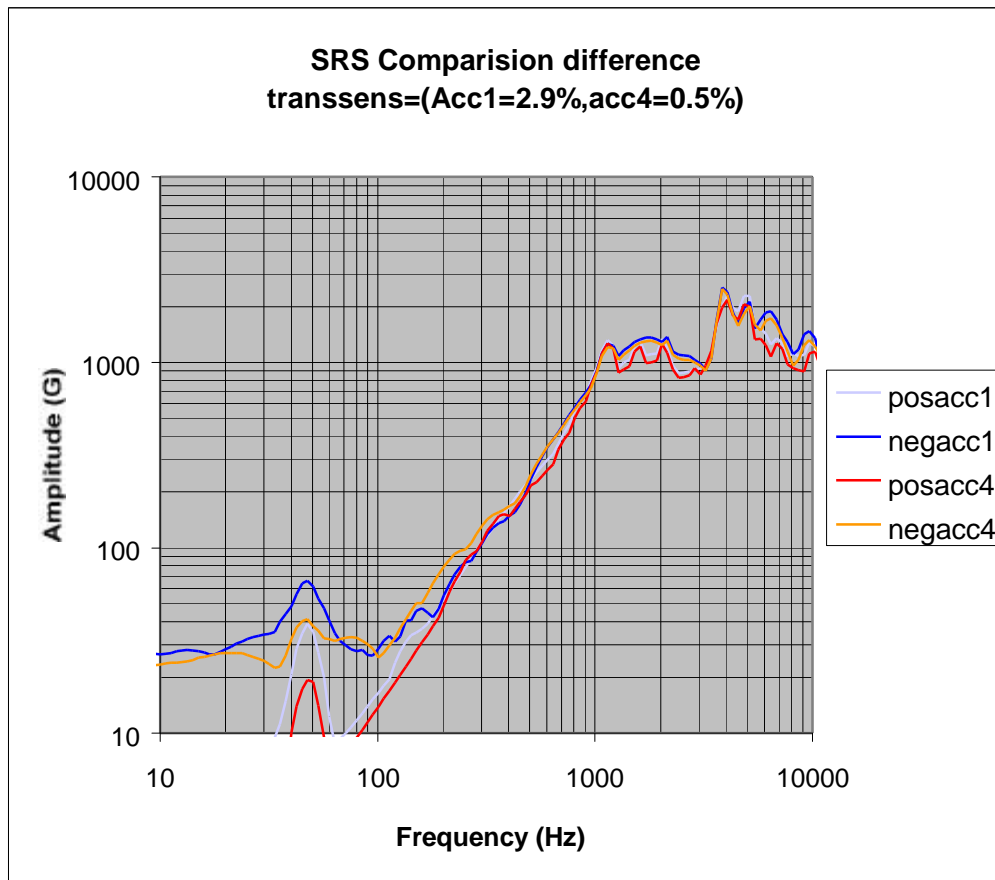


Figure 25: Comparison between accelerometers with different transverse sensitivities.

#### 6.2.4 The amplifier

A charge amplifier Beran model 602 was used. In the input setting the accelerometer's transverse sensitivity was typed. As an output setting, the input value you wish was chosen. If you choose 10 mV-g out must adjust your amplitude with a factor 100 in the Excel file. If you choose the other one 100 mV-g, the adjustment of the amplitude was 1000.

#### 6.2.5 Lecroy oscilloscope

An oscilloscope Lecroy 9354 was used. The oscilloscope measures the amplitude-time function. The following setup was used:

- The time/div=20 ms.
- Amplitude volt/div=2,0V.
- In the time base setup we use 50 000 samples at 250 kS/s (4µs/pt) for 200 ms.
- Record up to 50 k.

#### 6.2.6 Interface card

The interface card gives a opportunity to connect the PC with the oscilloscope. First an interface card called GPIB-PCIIA was used. No software routine was available for this interface card, so a HP interface card was used instead.

#### 6.2.7 Interface card software

An interface card connected the oscilloscope with a PC. The data are transferred with a software program called HP-VEE.

#### 6.2.8 Scangraph

Scangraph is a matlab program which converts the oscilloscope graph to an amplitude-time vectorfile.

- To succeed it's important to be in the current directory. For example **c:/exjobbpyro/srs.**
- To change directory: **cd c:/exjobbpyro/srs.**
- To call the program: **scangraph('accs.lc1', 'accs.txt');** There the first part is the outfile from the oscilloscope and the second one the resulting amplitude-vectorfile in text format.

#### 6.2.9 SRS-program

The most widely used technique for qualifying pyroshock is the Shock Response Spectrum (SRS). The SRS is a method of reducing the time-history to compare shock motions, to design equipment to withstand shocks, or to formulate laboratory test simulating environmental conditions.

## 7. MEASUREMENT OF PYROTECHNIC SHOCK

### 7.1 Repeatability

The test has to be repeatable when all the control parameters are the same. This is of primary importance. The difference between two test results has to be much lower than the test tolerances in at least two cases:

1. From test to test to allow the trial-and-error process but also to allow the performance of additional tests when several impacts at the same level are requested.
2. After dismounting of dummy and mounting of the test item.

In our SRS acquisition (figure 26) the two cases are almost achieved. The SRS graph show two measurements done during two different periods when the dummy and the triangular test fixture have been dismantled. The drop angle and accelerometer position is the same.

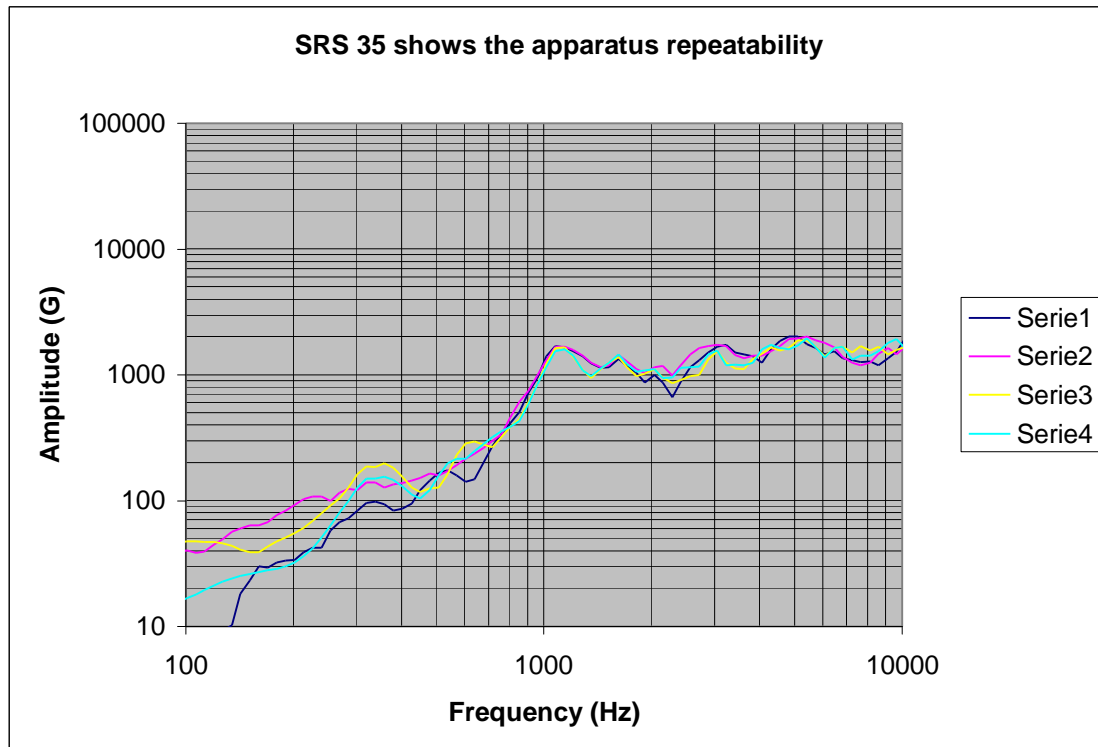


**Figure 26:** The apparatus repeatability is shown here. Series 1 is the first test positive curve, series 2 the first test negative curve. Series 3 shows the test 2 positive curves and series 4 the negative one.

## 7.2 Positive and negative SRS's

Note that the shock response spectrum is displayed in terms of its positive and negative spectral curves. They are used to check the SRS measurement quality. Ideally, the two curves should be approximately equal especially around the test specifications limit usually between 500 Hz-10000Hz.

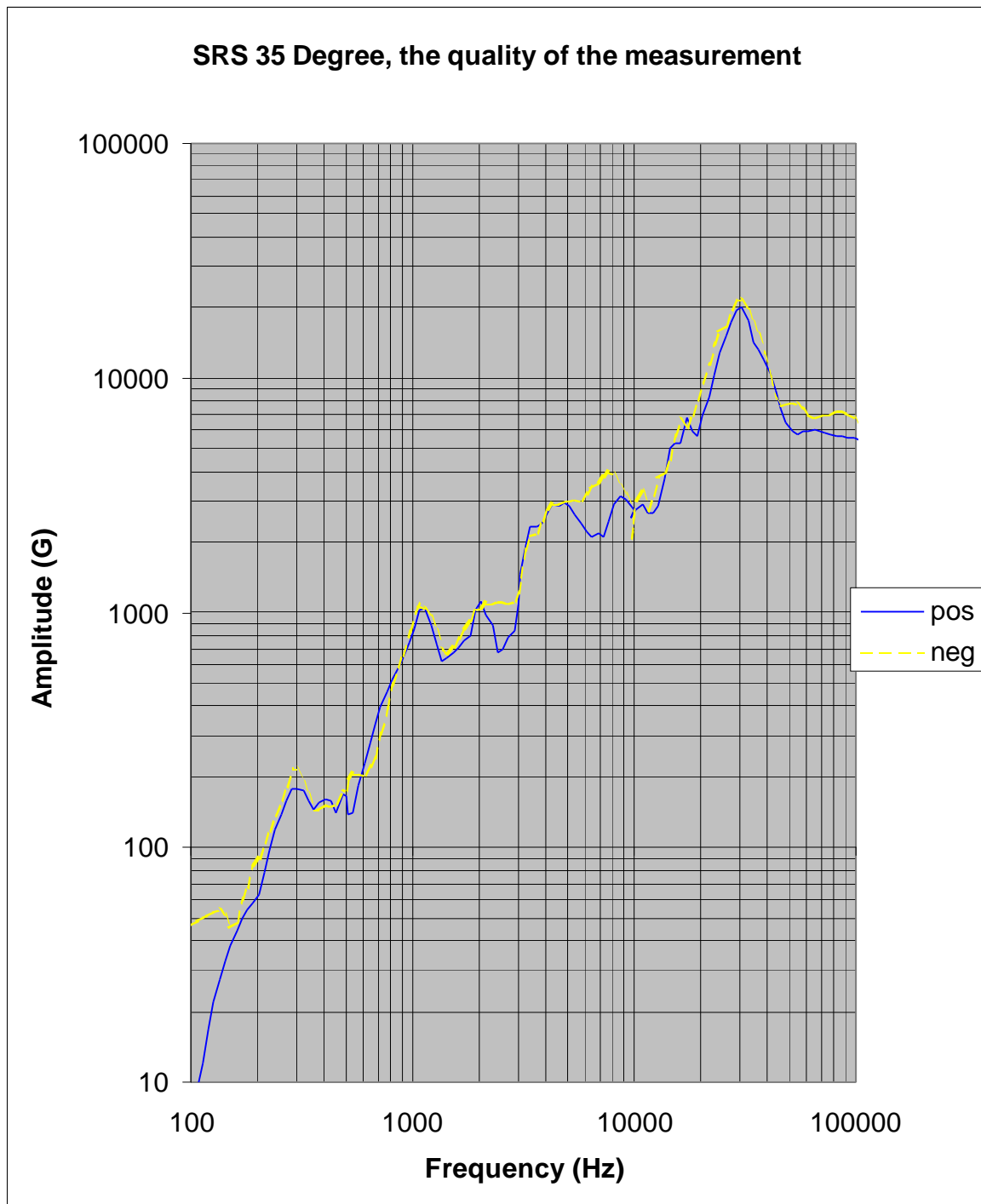


*Figure 27: A positive and negative SRS that are approximately equal.*

### 7.3 Changing the characteristics of SRS

For mechanical impact, the main parameters affecting the shock amplitude, shape and direction are the type of test fixture, the impact direction, the distance from impact point to test item, the anvil material, hitting tip material, the dropping mass weight and the drop height.

In the measurements the following parameters were changed:

- The drop angle,
- The hammer's weight,
- Using different damping material between the hammerhead and the impact surface,
- The distance from the impact to the test item,
- The mockup weight and
- Add damping clay on the fixture in specially chosen points

#### 7.3.1 Effect of changing of the drop angle

The figure 28 shows how the drop angle change the SRS characteristic. The SRS rise with bigger angle.

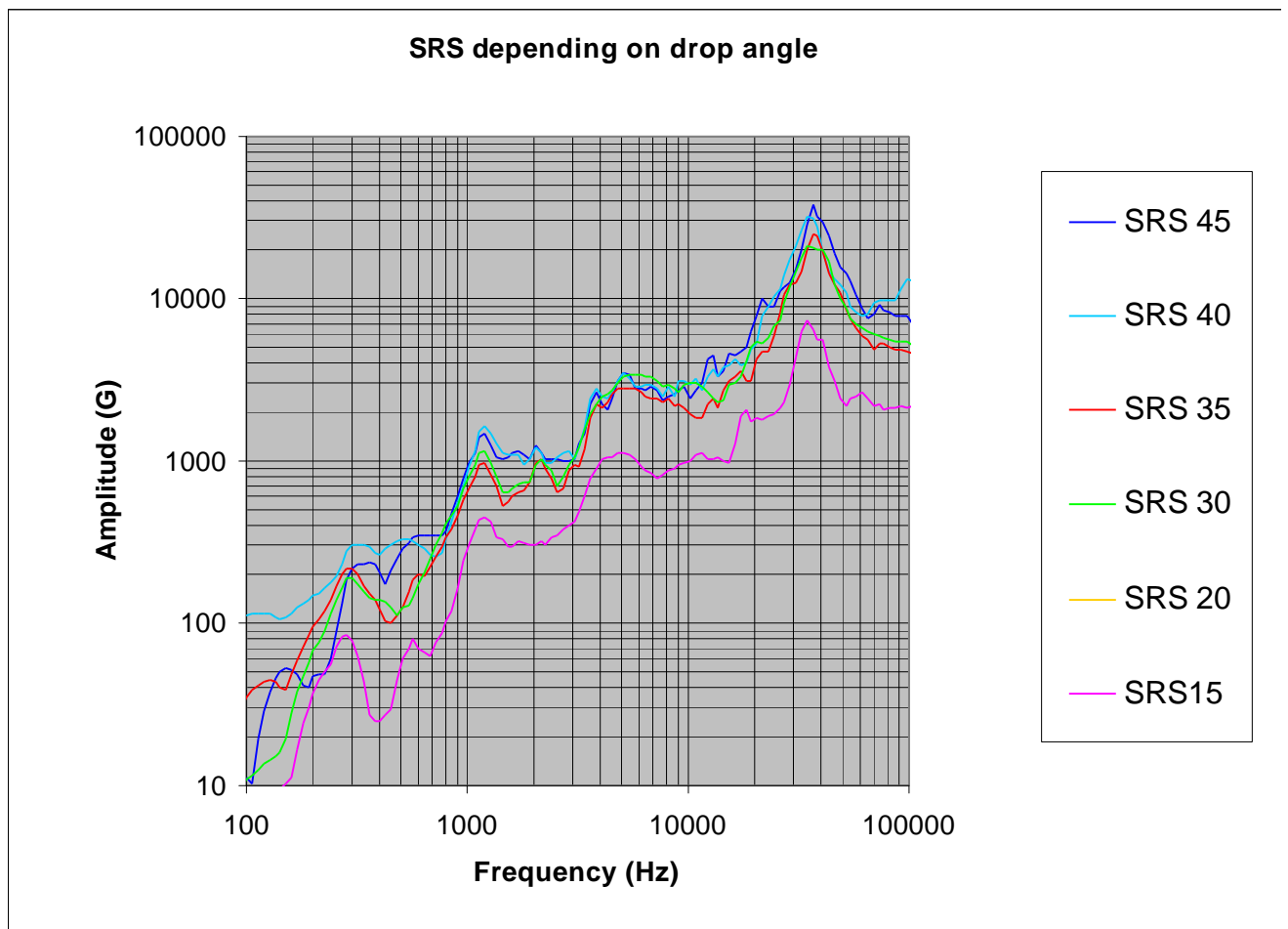


**Figure 28:** SRS depending on the drop angle measured with the protractor (in degrees).

### 7.3.2 Effect of changing the hammerweight

A modification to the prototype apparatus was to mount an adjustable weight system. The mass of the impact hammer was changed by add barrel weights. When a weight of 5 kg was added, the characteristic wasn't change to much. This weight gives a good opportunity to fine adjust the SRS curve.

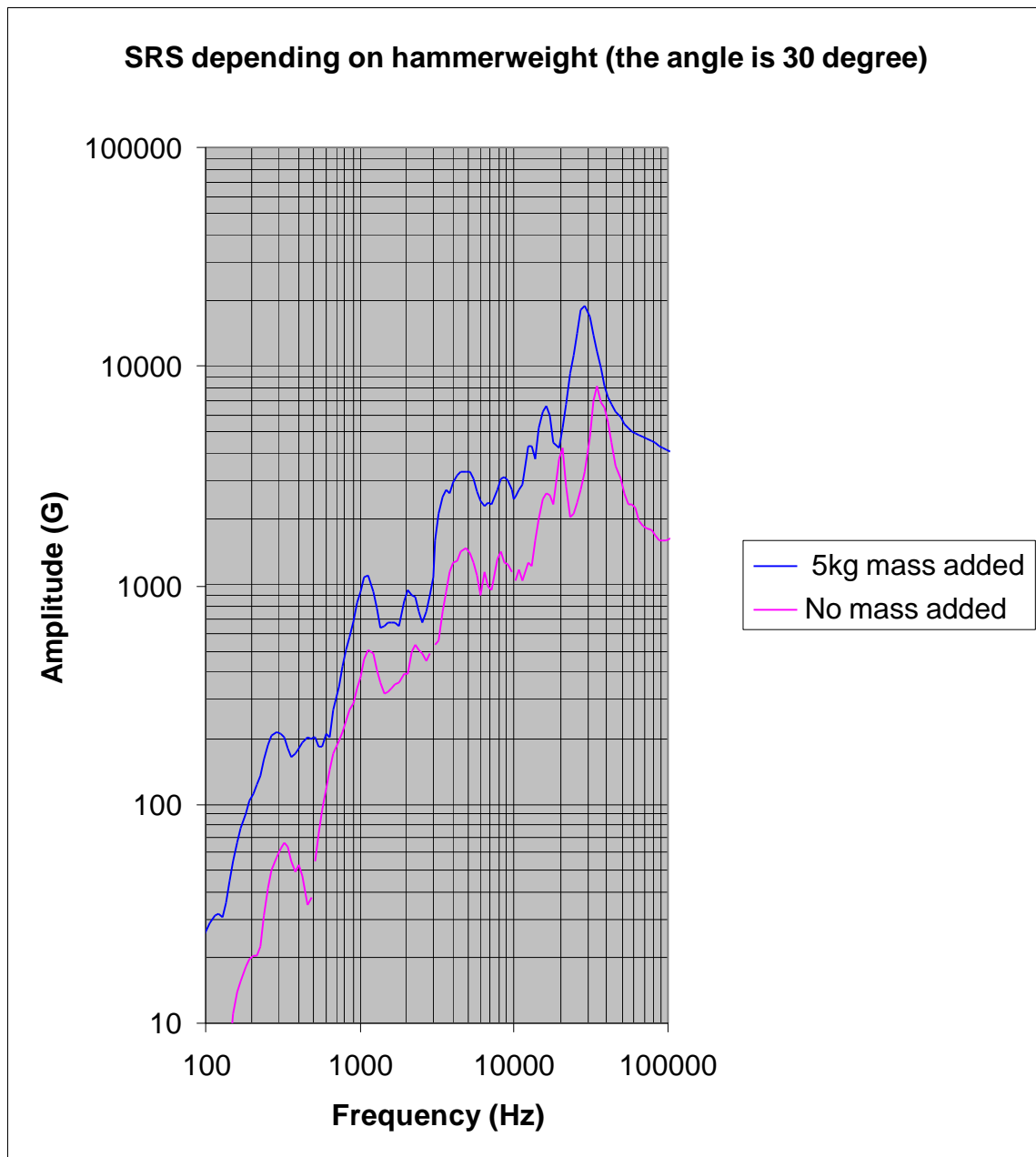


*Figure 29: SRS curve depending on hammerweight*

### 7.3.3 Effect of using damping between the hammerhead and the impact surface

A lot of different sylomer damping material was used, but this material gave too much damping and too low a SRS graph. Better SRS characteristic gets with 10 or 20 pieces of paper, which working as damping. The graph below shows the results of adding a little damping if you want to bring the high frequency end down. The drop angle and hammer mass were constant during the test.

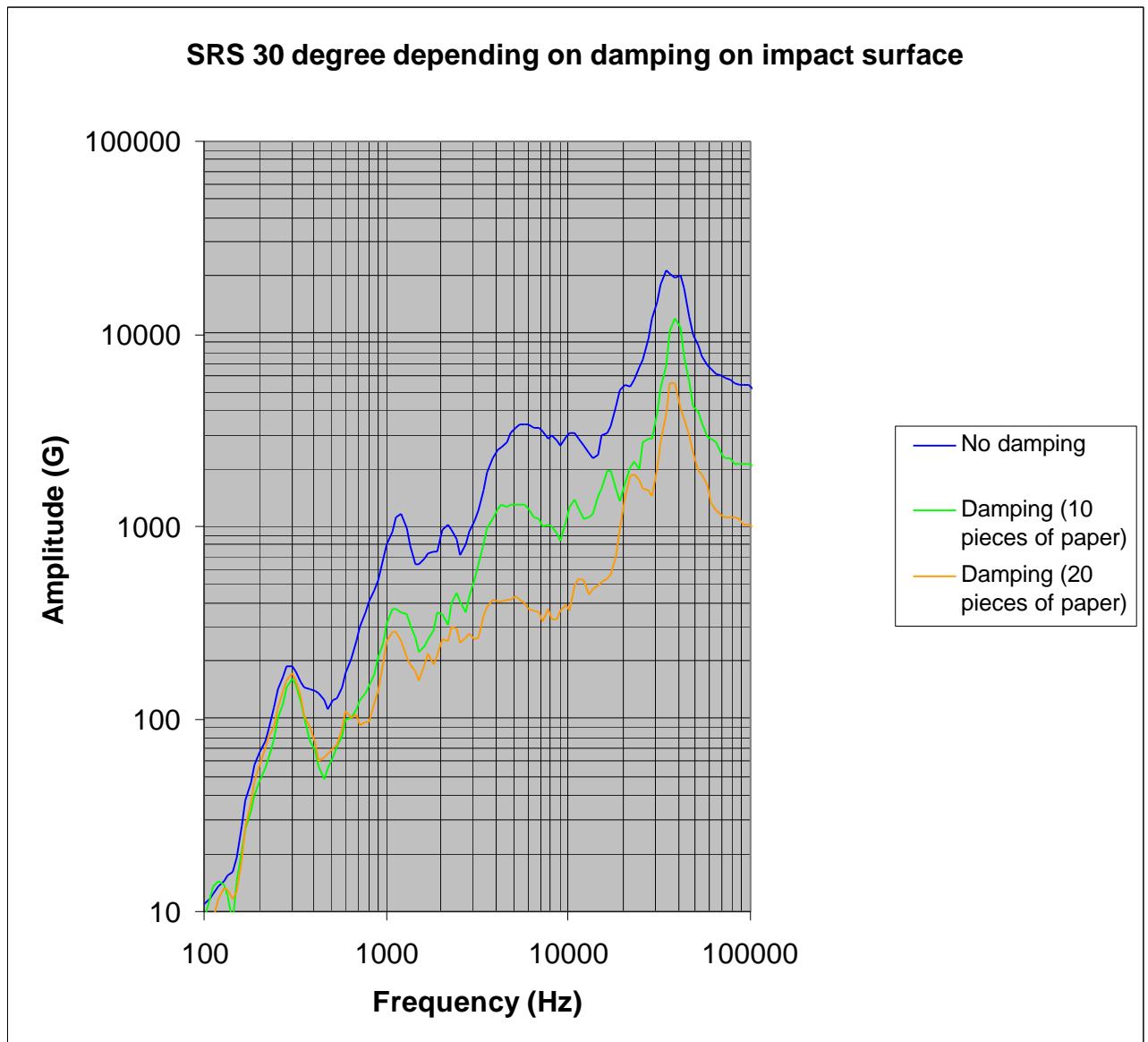
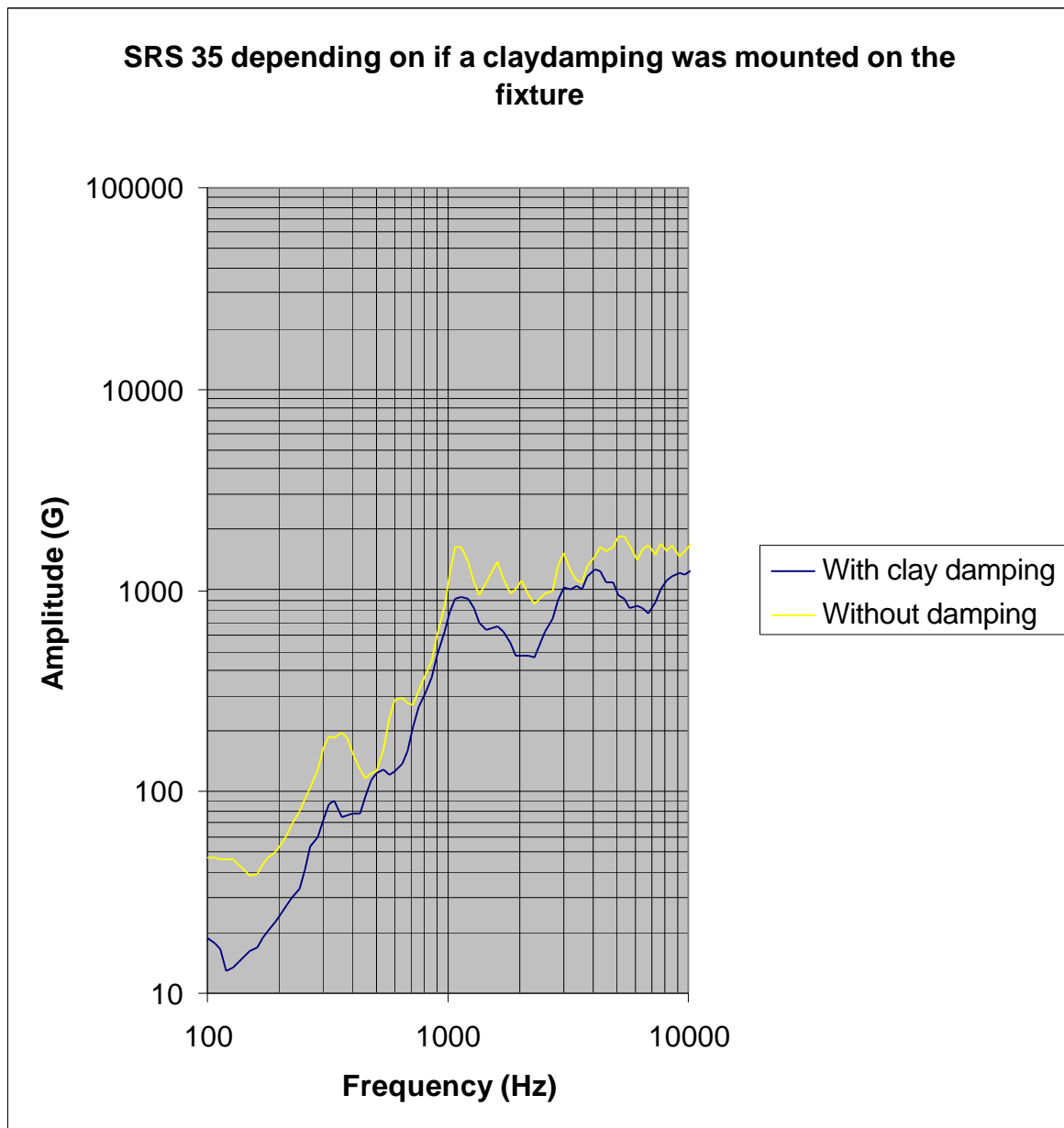


Figure 30: Effect of change in damping on the SRS.

### 7.3.4 Effect of using clay damping on the fixture

In the figure 31, a comparison of measuring with and without clay damping was shown. No movement of the knee frequency was reached. But the SRS amplitude decreases in the whole frequency domain.



**Figure 31:** SRS depending on if we add clay damping on the fixture.

### 7.3.5 Effect of changing the weight of the mockup

A mockup is a model of a computer box. What is happening with the shape of the SRS, if the weight of the mockup is changing? Firstly a test with a mockup with the mass of 9,7 kg was done and then we added a mass of 9,2 kg and do a comparison (see figure 32).

The results agree with the theory. A mass placed on the fixture gives a mass damping and a rise in the SRS curve.

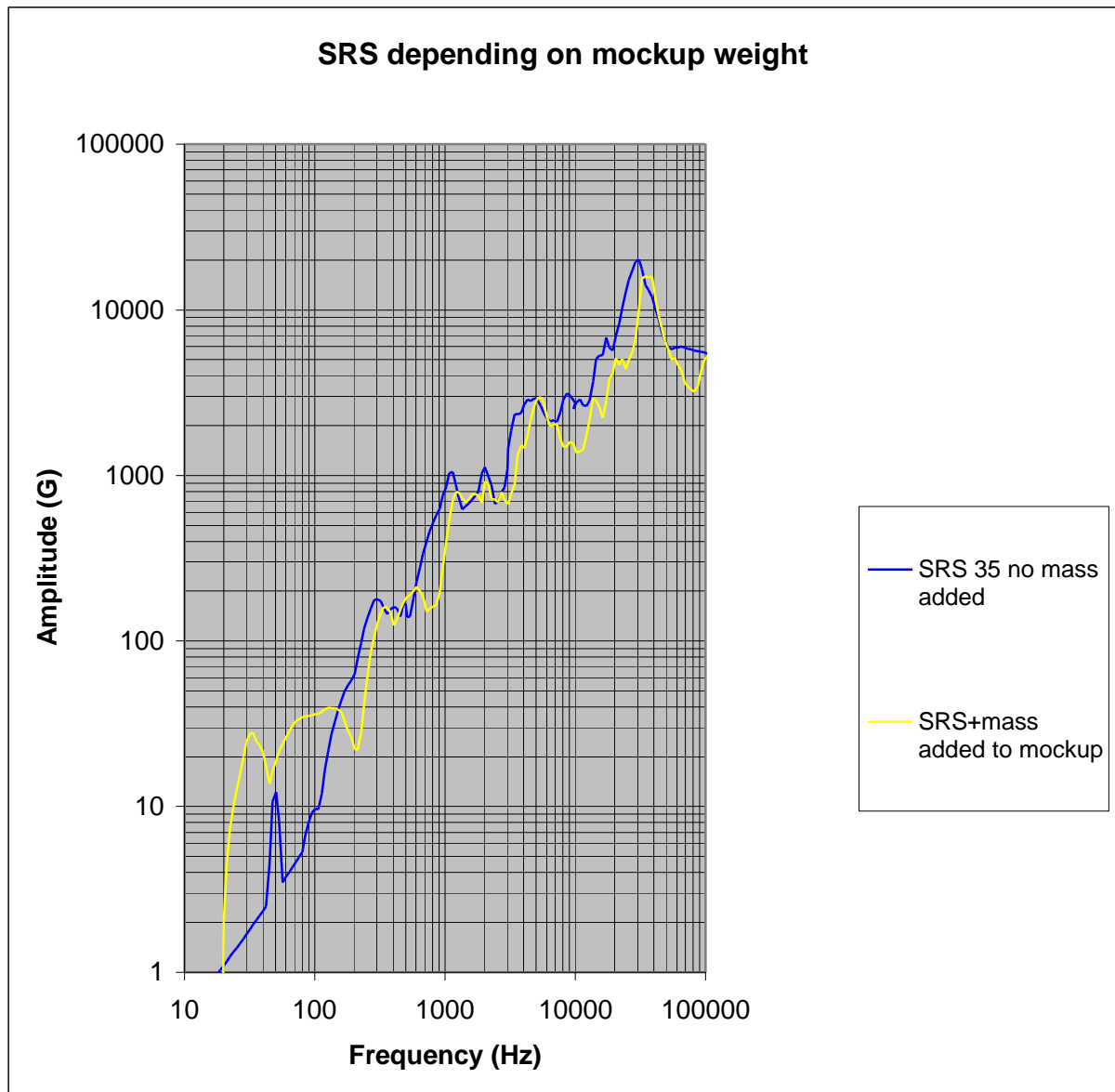
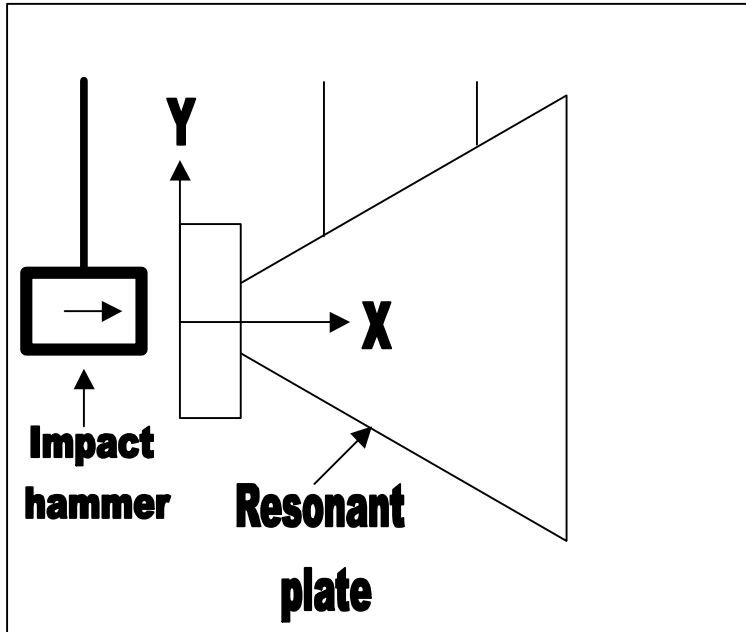


Figure 32: SRS depending on the weight of the mockup.

### 7.3.6 Effect of changing the distance from the impact to the test item

A lot of measurements have been done to see how the distance from the impact to the accelerometer affects the SRS. The fixture was marked up with a coordinate system (see figure 33).



*Figure 33: The coordinate axes on the fixture*

From figure 34 to figure 36 some really interesting observation was done.

- The measurement in the nearfield  $X < 20$  cm gives us badly accuracy in the low frequency, the positive and negative curves correspondence is poor (see figure 36).
- The SRS get a higher value if the accelerometer is placed near the edge of the fixture. The reason for this is that the wave is reflected and reinforces the amplitude.
- On this fixture only small test objects could be mounted. Large objects will be affected by the edge reflection phenomenon.
- The analysis of the fixture modes and how they affect the amplitude will be explained further on.

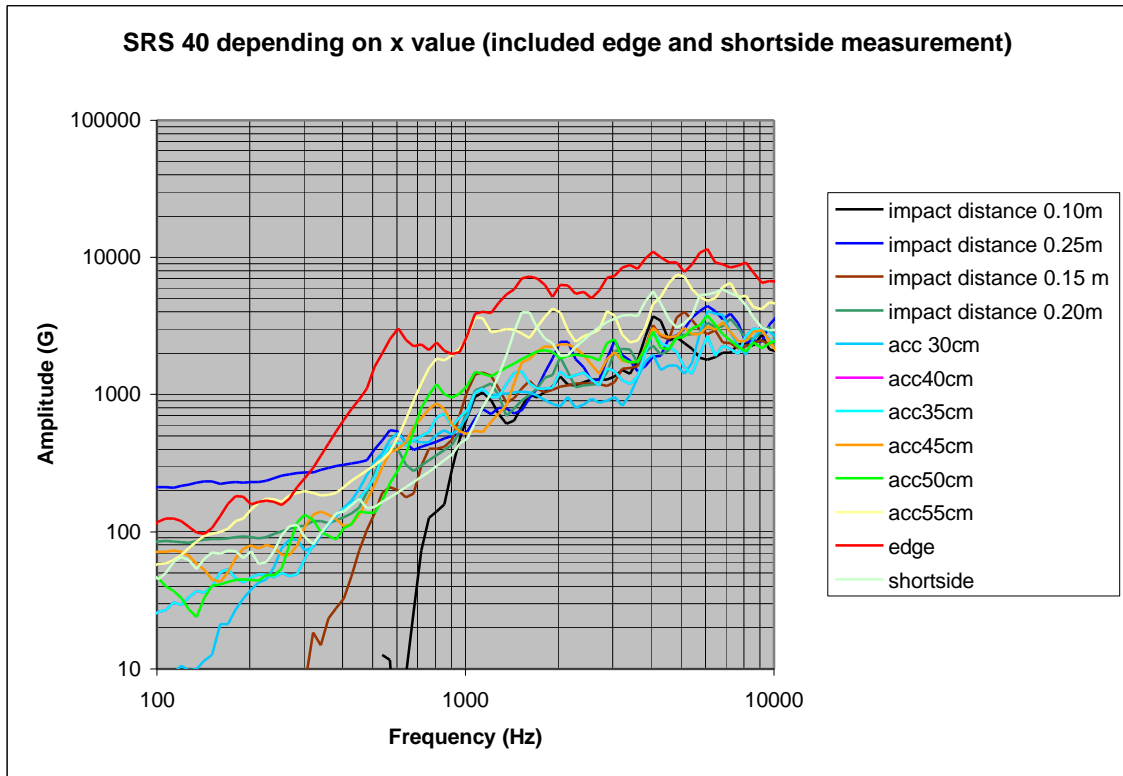


*Figure 34: SRS depending on the distance to the impact. The y value constant ( $y=0$ ).*

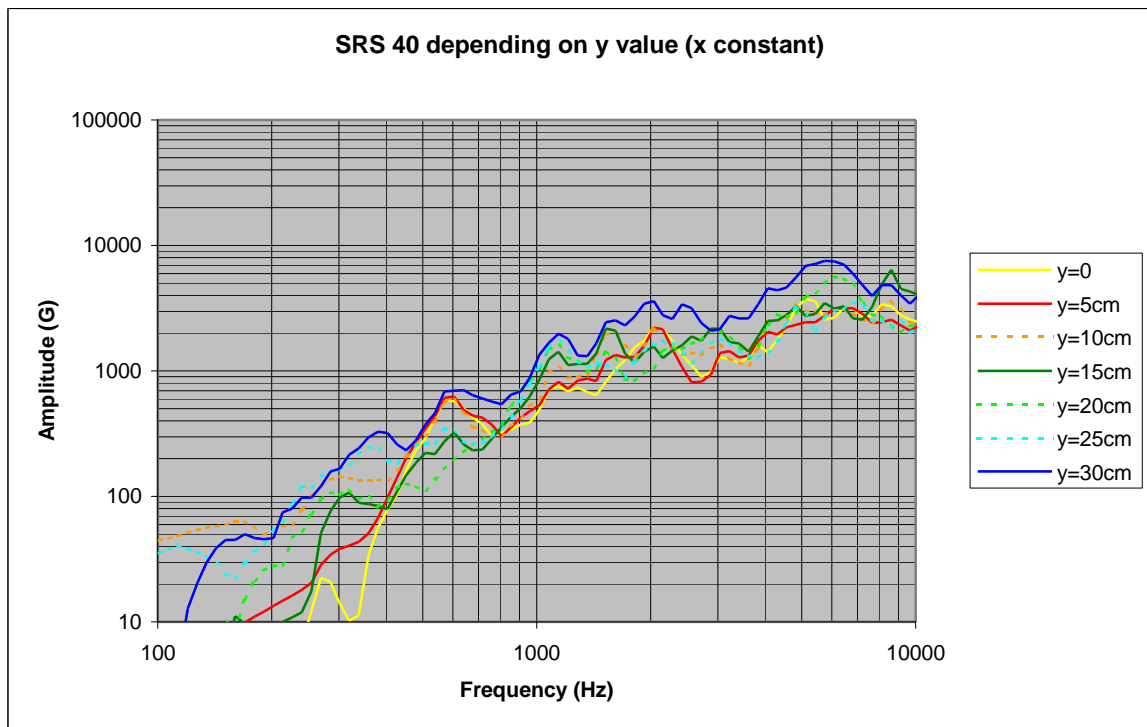


*Figure 35: SRS there the y value is changed. The x value is constant ( $x=25$  cm).*

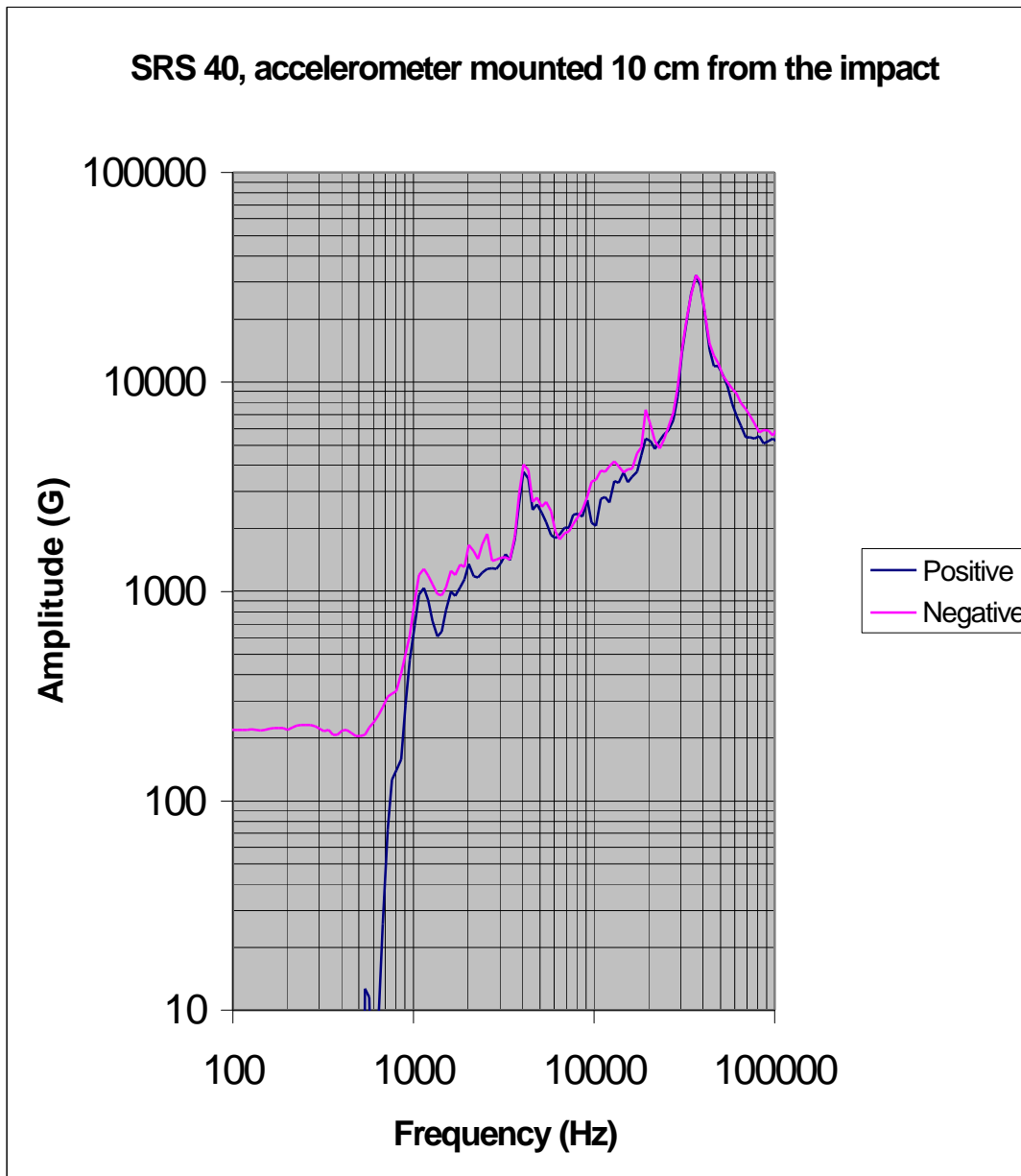


*Figure 36: Poor correspondence between the positive and negative curve.*

## 8. A comparison with a drop table test

Saab Ericsson Space has carried out a pyrotechnic test for the specific computer for use in commercial satellites. Their test apparatus is an old-fashioned drop table. The figure 37 shows the shock requirement from the customer. The tolerance is 3 dB.

Frequency (Hz)	Shock Response (Q=10) Qualification level (G)
200	50
400	100
1400	350
1600	350
4000	300

*Figure 37: Table Shock levels for the computer test.*

The accelerometer was placed at the foot of the mockup. In the figure 38 below the result from the drop table is inserted so a comparison can be done with the resonant plate measurement. The measurements were done with a drop angle of 30 degrees and a damping of 5 pieces of paper to fit the tolerance level.

The result shows that Saab Ericsson Space can easily do tests like this with their prototype pyroshock apparatus.

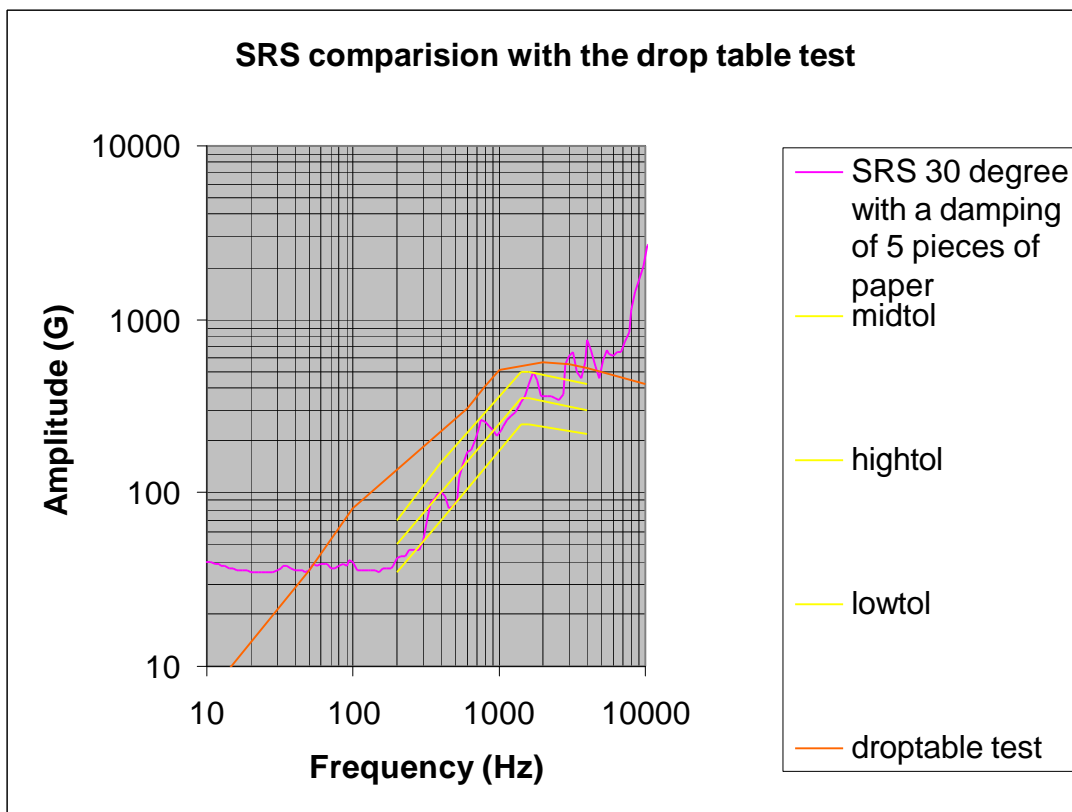


*Figure 38: Comparison between our SRS measurement and the drop table test*

## **9. Analysis of the fixture**

To investigate if there is a simple connection between our SRS and, primary, the lowest bending modes was an analysis of the excitation plate done.

The computer program ANSYS54 was used to perform the analyses, and the measurement where made in the Department of Applied Acoustics, Chalmers.

### **9.1 Mobility measurement**

A simple method is to use hammer excitation.

The test equipments which was used:

- A impact hammer of the model Brüel & Kjær type 8202 (ser No 1225787)
- A Genrad FFT analyser.
- A Brüel & Kjær (typ 2626)amplifier.

The hammer, by itself, is the excitation mechanism and is used to impact the structure and thus excite a broad range of frequencies. The Genrad FIF real time analyzer received the signal from the impact hammer and accerelation from the accelerometer. The result in figure 40 shows a magnitude-frequency graph.

An analysis of the three first modes 165 Hz, 244 Hz and 323 Hz was done.

To get the fixture modeshape, measurement for different points must be done.

Impacts in 35 decided point on the fixture was done and coordinates, magnitudes and phaseinformation was used in a matlab animination program. The mode shapes are shown in the figure 42-44.

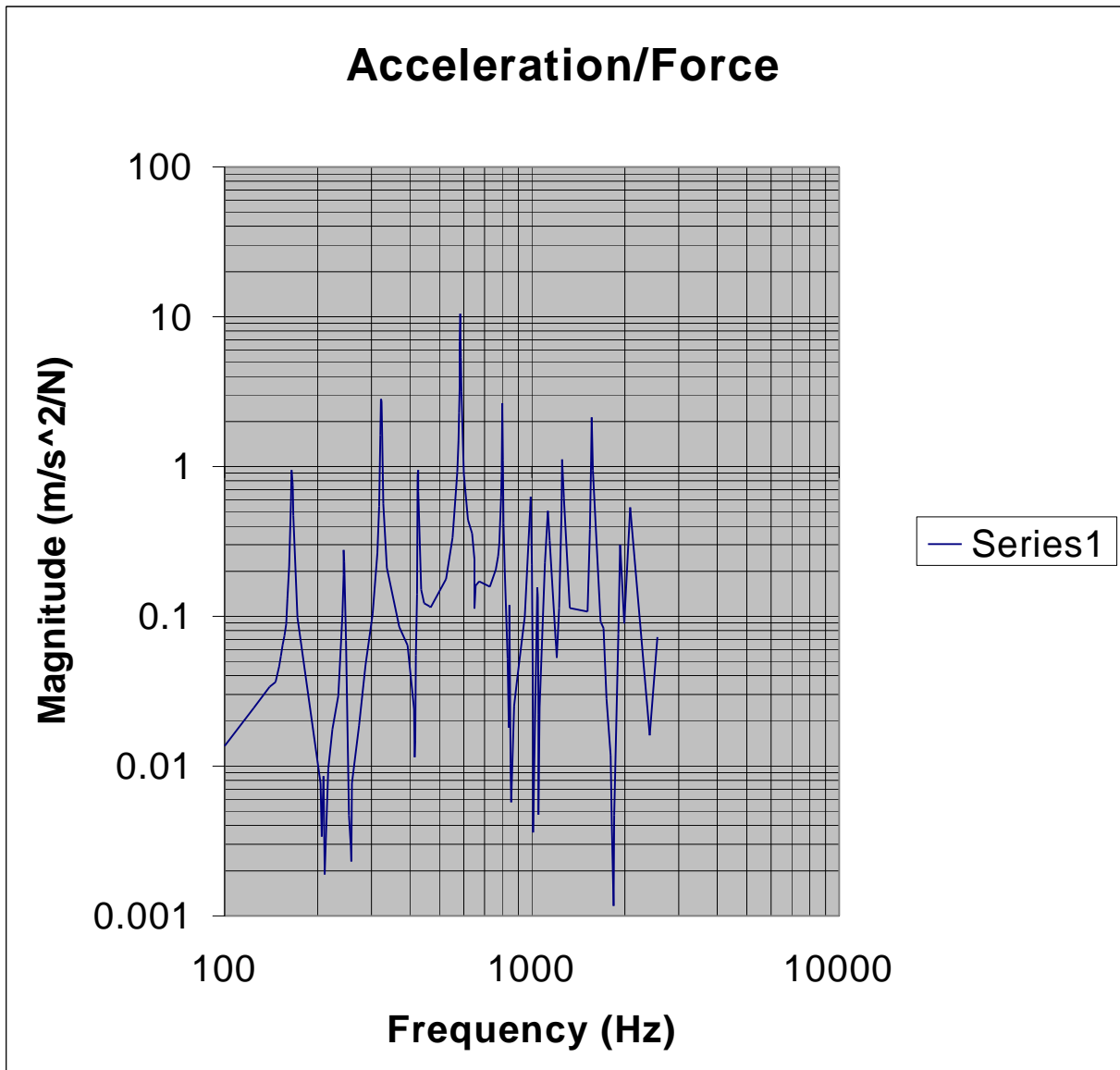


*Figure 40: The mobility curve shows the eigenfrequencies of the fixture*

## 9.2 FEM analysis of the fixture

One problem with analysing this plate is the rigid body modes. The plate is considered to be without support, because it is in reality hanging from two wires and this *system* has much lower frequencies than the first bending modes.

That means, that the highest of the six rigid body moves has to be much lower than the first bending mode, not to influence the analysis. An example of a rigid body motion is shown in fig 41.

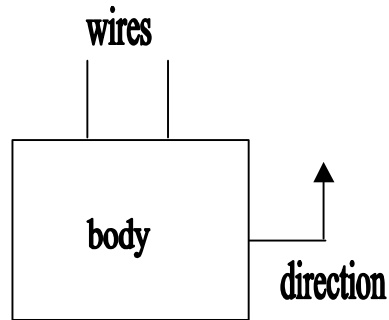


*Figure 41: Rigid body motion.*

If the wires are too stiff, they will affect the first bending modes. Due to the chosen boundary conditions (no support), ANSYS54 will give the first six rigid body modes. In other words  $f_{1...6} = 0$  Hz, the first six eigenfrequencies will be 0.

## 9.3 The fixture's mode shapes

In the left part of 42 a modeshape from a FE calculation is shown. The corresponding eigenfrequency was calculated to 184 Hz.

The matlab animation program shows the first measured mode at 165 Hz (see right part of 42). This mode was measured with a mobility measurement.

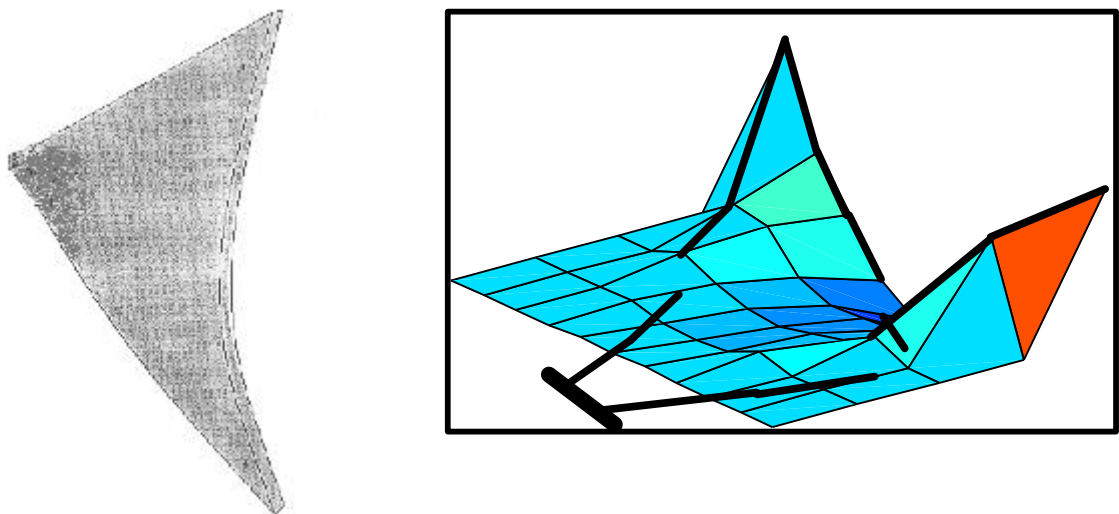


*Figure 42: Left: First mode with frequency 184 Hz calculated by the FEM . Right: First mode with frequency 165 Hz, evaluated by mobility measurement.*

The second mode shape is found at about 244 Hz (see figure 43) in the mode analysis. The result in the FE analysis is 256 Hz.

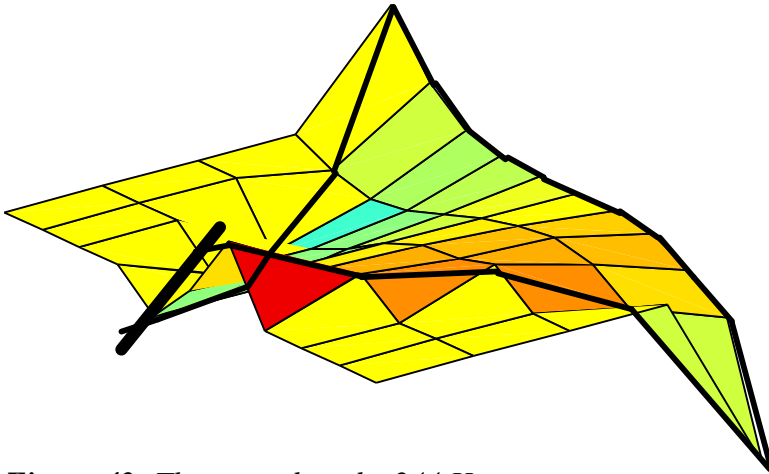


*Figure 43: The second mode, 244 Hz.*

The third mode had a eigenfrequency of 323 Hz (se figure 44). Mode shapes above these frequencies are more complex and are difficult to analyse in this matlab animation program. The FEM program calculated a similar mode shape with 378 Hz.

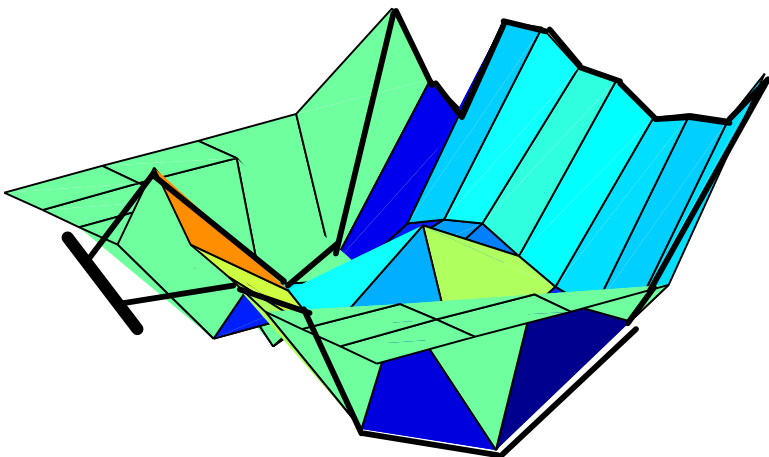


*Figure 44: Third mode, 323 Hz*

## 10. Conclusions of the fixture analysis

The frequencies from ANSYS54 are slightly different from the measured ones. Possible error sources:

- The exact values of the material parameters is unknown, typical values are used.
- The geometric shape of the model is not perfect. A change of the thickness of the plate,  $\Delta t = 0.7\text{mm}$  results in a theoretical change of the first bending mode about 10 Hz. The frequency is strongly depending on thickness. (Appendix C)
- In reality the wires influence the modal results slightly.

At first a triangular plate was analysed, but the model was too simple. Then a reinforcing left part and a added non-structural masses was included. The masses were set to the same value as the weight of the screws in the upper and lower right corner. The modes from the analysis and measurement are matching perfect, so it is really the shape of the first three bending modes we found. We can not find a simple connection between our SRS and the lowest bending modes.

## 11. ANALYSIS OF TEST ITEM

### 11.1 Theory used by ANSYS

The procedure employed for the solution is the Newmark time integration method. I.e the approximations [15]:

$U'_{n+1} = U'_n + [(1-\delta)U''_n + \delta(U''_{n+1})]\Delta t$  and  $U_{n+1} = U_n + U'_n\Delta t + [(1/2-\alpha)U''_n + \alpha(U''_{n+1})]\Delta t^2$  is used. The Newmark method is an implicit, conditionally stable integration scheme (Appendix B).

$\alpha, \delta$  = Newmark integration parameters.

$\Delta t = t_{n+1} - t_n$

$F^n$  = Applied load vector

$U_n$  = nodal displacement vector at time  $t_n$

$U'_n$  = nodal velocity vector at time  $t_n$

$U''_n$  = nodal acceleration vector at time  $t_n$

$U_{n+1}$  = nodal displacement vector at time  $t_{n+1}$

$U'_{n+1}$  = nodal velocity vector at time  $t_{n+1}$

$U''_{n+1}$  = nodal acceleration vector at time  $t_{n+1}$

The equation of motion at time  $t_{n+1}$ :

$$[M] U''_{n+1} + [C] U'_{n+1} + [K] U_{n+1} = F^a \dots(1)$$

By using the approximations (1) can be written as:

$$a_0M + a_1C + KU_{n+1} = F^a + M(a_0U_n + a_2U'_n + a_3U''_n) + C(a_1U_n + a_4U'_n + a_5U''_n) \dots(2)$$

As the Newmark method is conditionally stable it requires

$$\alpha \geq 1/4(1/2 + \delta)^2 ; \delta \geq 1/2 ; 1/2 + \delta + \alpha > 0$$

ANSYS54 selects values for the Newmark parameters as

$$\alpha = 1/4 (1/2 + \delta)^2 ; \delta = 1/2 + \gamma \text{ where } \gamma = \text{amplitude decay factor, in ANSYS defaulted to } 0.005.$$

### 11.2 Problem description

The aim is to perform a pyroshock analysis on a test mockup in ANSYS and to compare the result with measured values. Two different analyses are performed, one including the whole test item and the other using only the circuit board.

Different measured SRS is used as input.

### 11.2.1 Material data

Following material data is used in the analysis of the test mockup:

Material	Density [kg/m <sup>3</sup> ]	Poisson's ratio	Young's modulus [N/m <sup>2</sup> ]
Aluminium	2700	0.3	70*10 <sup>9</sup>
Polyimide (PCB)	1800	0.15	28*10 <sup>9</sup>

### 11.3 Available methods

Three methods of solution are available [14]:

- Full integration method
- Reduced integration method
- Mode superposition

The full integration method solves (2) directly and makes no additional assumptions. Nonlinearities may be included. The main drawback is the cost of the analysis.

The reduced integration method uses reduced structure matrices to solve the time dependent equation of motion for linear structures. Restrictions and assumptions:

1. Constant mass- [M], damping- [C] and stiffness- [K] matrices imply no large deflections, no change of stress stiffening, no plasticity, no creeping nor swelling.
2. Constant time step size in the time integration.
3. No element load vectors, only nodal forces applied directly at master degree of freedom (MDOF) or acceleration effects acting on the reduced mass matrix are permitted.
4. Non-zero displacement may be applied only at the master DOF.

The method runs faster than the full transient dynamic analysis. The master degrees of freedom is the essential DOF:s required to characterise the response of the system. The total number of MDOF should be at least twice the number of modes of interest.

The mode superposition method uses the natural frequencies and modeshapes of a linear structure to predict the response to transient forcing functions. Restrictions and assumptions:

1. Constant mass- [M], damping- [C] and stiffness- [K] matrices imply no large deflections, no change of stress stiffening, no plasticity, no creeping nor swelling.
2. Constant time step size
3. There are no element damping matrices. However, various types of system damping are available.
4. Time varying imposed displacements is not allowed.

The mode superposition method accepts modal damping (damping ratio as a function of mode number). If a single point response spectrum analysis is to follow – damping can be specified in a non-damped model analysis. The damping will then not affect the eigenvalue solution. It is used to calculate an effective damping ratio for each mode, which is then used to calculate the response spectrum. Spectrum analysis is explained below.

Damping choices:

- Alpha (Mass) damping [ALPHAD]
- Beta (Stiffness) damping [BETAD]
- Constant damping ratio [DMPRAT]
- Material depending damping ratio [MP,DAMP]

The mode superposition method is chosen because the complexity of the model and the required small time step. The constant damping ratio 5% is used here, (approximate value from measurement).

### 11.3.1 Spectrum analysis

A spectrum analysis is an analysis where the results of a model analysis are used with a known spectrum to calculate displacements, velocities, accelerations and stresses in the model.

The spectrum is a graph of spectral values versus frequency that captures the intensity and frequency content of time-history loads. There are three types of spectra available for spectrum analysis [14]:

- Response spectrum
- Dynamic Design Analysis Method (DDAM)
- Power Spectral Density (PSD)

A response spectrum represents the response of single-DOF system to a time history loading function. It is a graph of response versus frequency, where the response might be displacement, velocity, acceleration or force. One could choose between single-point response (SPRS) spectrum and multi-point response spectrum (MPRS). In a SPRS analysis, one specifies one response spectrum curve at a set of points in the model, such as all supports. In a MPRS analysis, one specifies different spectrum curves at different sets of points. Up to ten different simultaneous input spectra is allowed in ANSYS54.

The dynamic design analysis method is a technique used to evaluate the shock resistance of shipboard equipment. The technique is essentially a response spectrum analysis in which the spectrum is obtained from a series of empirical equations and shock design tables provided in the U.S Naval research laboratory report NRL-1396.

A power spectral density spectrum is a statistical measure of the response of a structure to random dynamic loading conditions and is used in random vibration analysis.

Measurement shows that the input spectrum looks different depending on location. Despite this fact the SPRS is used to simplify the analysis.

## 11.4 Solid or plate theory model

To use plates instead of solids will result in a shorter computation time.

Consider a free supported rectangular plate. In Appendix C it is shown that

$$\omega = \pi^2 [r^2/a^2 + s^2/b^2] \sqrt{D/m}.$$

Where a and b are the side length of the rectangle and D, m constants given in Appendix C. r and s are integers depending on mode number.

Let a = 1m, b = 0.5m, t = 0.005m,  $\nu = 0.3$  and E = 210 GPa. Then the first mode will occur when

r = s = 1. The frequency are given by  $f_i = \omega_i/2\pi$ .

The table below summarises the results.

	Time	$f_1$	$f_2$	Numbers of element
Analytical	--	22.2 Hz	35.6 Hz	--
Plate model	25 s	22.2 Hz	35.5 Hz	325
Solid model	1 min 9 s	22.2 Hz	35.5 Hz	325

The time waste in solid modelling is clear. It is important to use proper element geometry. If one uses the tetraeder instead of rectangle in the analysis above, the solution time increases to approximately 10min, mainly because it takes 3100 elements to avoid create degenerated shapes.

## 11.5 Mainsteps in the analysis

1. Build the model
2. Obtain the modal solution
3. Obtain the spectrum solution
4. Expand the modes
5. Combine the modes
6. Review the result.

### 11.5.1 Combination of modes

ANSYS offers five different mode combination methods for the single-point response spectrum analysis [15]:

- Square Root of Sum of Squares (SRSS)
- Complete Quadratic Combination (CQC)
- Double Sum (DSUM)
- Grouping (GRP)
- Naval Research Laboratory Sum (NRLSUM)

These methods generate coefficients for the combination of mode shapes. This combination is done by a generalisation of the method of the square root of the sum of the square. I.e:

$$R_a = [\sum_i \sum_j \in_{i,j} R_i R_j]^{1/2} \quad \text{where } i = 1 \dots N \text{ and } j = 1 \dots N$$

$R_a$  = total modal response

$N$  = total number of expand modes

$\in_{i,j}$  = coupling coefficient. (Depending on chosen method)

$R_i = A_i \Psi_i$  = modal response of the  $i$ :th mode

$R_j = A_j \Psi_j$  = modal response of the  $j$ :th mode

$A_i$  = mode coefficient for the  $i$ :th mode

$A_j$  = mode coefficient for the  $j$ :th mode

$\Psi_i$  = the  $i$ :th mode shape

$\Psi_j$  = the  $j$ :th mode shape

For example, the GRP method uses

$$R_a = [\sum_i \sum_j \in_{i,j} |R_i R_j|]^{1/2} \quad \text{and } \in_{i,j} = 1 \text{ if } (\omega_j - \omega_i)/\omega_i \leq 0.1 \text{ else } 0$$

The SRSS

$$R_a = [\sum_i (R_i^2)]^{1/2}$$

The NRL sum

$$R_a = |R_{a1}| + [\sum_i (R_{ai})^2]^{1/2} \text{ where } i = 2 \dots N \text{ here.}$$

$|R_{a1}|$  = absolute value of the largest modal displacement, stress or reaction at that point.

$R_{ai}$  = displacement, stress or reaction contributes of the same point from the other modes.

The calculation where performed using the NRL sum.

In some of the mode combinations the damping is included in calculation of  $\in_{i,j}$ .

## 11.6 Conclusion of mockup test analysis

A measured SRS where used as spectral input. Following the main steps given in 11.5 with material data according to 11.2.1 results in: ( $g$  is the gravity constant,  $[m/s^2]$ ).

Measured values [g]	Whole model [g]	Input direct to circuit [g]
2000	3040	2850

The values from the analysis are much higher than the measured ones. The conclusion is: Using the SRS as input in a modal analysis will result in an over conservative test when the NRL sum is used in the combination of the modes.

The result is also sensitive to assumed damping, which is here received through measurement. Frequency content up to 1521 Hz where included in the analysis. The analysed test fixture is containing only one circuit board. To analyse a complete computer will be even more difficult because many more modes need to be included to reach the same frequency content as in the simple model.

## **12. CONCLUSIONS**

### **12.1 Conclusions**

The pyroshock apparatus has a good repeatability and ability to change the characteristics of SRS. To shift the kneefrequency another fixture has to be used.

Receiving the SRS output with the existing test facilities was complicated. An FFT-analysator will do the measurement more quickly and conveniently.

Today's shock test, which earlier has used the drop table test method, is possible to do in the pyroshock apparatus.

The SRS provides a simple conservative test, which is commonly used. For the used fixture there wasn't a simple connection between the kneefrequency in the SRS and the first bending modes. One analysis in ANSYS and one mobility measurement was done to determine the lowest bending modes.

When performing a pyroshock analysis both the finite element method (FEM) and statistical energy analysis (SEA) suffers from drawbacks. An attempt to combine these two methods is under development. The coming program, AutoSEA2, will offer SRS outputs.

Using a measured SRS as input in a mode superposition analysis in ANSYS could result in an over conservative test. To analyse pyroshock events using FEM is difficult because some parameters, such as damping, have to be measured and the analysis demands a great deal of computer power.

### **12.2 Further Work**

Different test fixtures might be developed to match the new requirements. The magnitude and shape can also be changed with different shock testing devices. A study of air gun impact and explosive impact are interesting in a further work (see reference 6 for more information about these testing devices).

The set-up time and the cost will be reduced if the experience and measurement results are inserted in a database.

An analysis performed with AutoSEA2 compared with actual levels from measurement would be of great interest.

A more convenient way to handle damping parameters should be developed when dealing with analyses.

### 13. References

- [1] Dave S. Steinberg: "Vibration Analysis For Electronic Equipment" 2<sup>nd</sup> ed. USA, 1988, pp.324-325.
- [2] Cyril M. Harris: "Shock and Vibration Handbook" 4<sup>th</sup> ed. USA, 1995, chapter 26 pp 24-34.
- [3] R.G Meritt: "Test Technology", The Shock and vibration digest: a publication OCT 01 1989 v 21 n10.
- [4] Robert E. Morse: "Comparision of response from different resonant plate simulation techniques", Shock and Vibration Bulletin 56 part 3, Aug 1986, pp 85-116.
- [5] C.J. Litz, Jr., P.E: "Laser Doppler Vibrometer, Unique use DOE/TAGUCHI methodlogies in the arena of pyroshock (10 to 100000 Hz) response spectrum" USA, 1994, Proceedings of SPIE – The international Society for optical Engineering First Int. Conference on Vibration Measurements by Laser Techniques, vol 2358, pp 432-449.
- [6] E. Filippi, "Development of the Alactel ETCA pyroshock test facility" Proceedings European Conference on Spacecraft Structures, Materials and Mechanical Testing, SP-428, Stadthalle Braunschweig Germany 4-6 November 1998, pp. 677-687, ISBN 92-9092-712-7.
- [7] Tom Irvine: "An Introduction to the Shock Response Spectrum", Arizona State University. This article is publised in Tom Irvines homepage (tutorial) see: [www.vibrationdata.com](http://www.vibrationdata.com).
- [8] Fashin Craig Chang, Thomas L Paez, Fredrick Ju, "Least favourable response of inelastic structures",. The University of New Mexico, Albuquerque, NM 87131.
- [9] Dave S. Steinberg, "Vibration analysis for electronic equipment" 2<sup>nd</sup> ed. 1988, USA, pp 275-326.
- [10] Klaus-Jürgen Bathe, "Finite element procedures" Englewwod Cliffs,N.Y:Prentice Hall,cop1996, ISBN 0-13-301458-4
- [11] Jan Petersson, "Matematisk Analys 2", Hisingskärä, cop 1996, ISBN 992-036065-1
- [12] Jens Trampe Broch, "The application of the Brüel&Kjaer measuring systems to mechanical vibration and shock measurements", Naerum 1969, ISBN 99-0102346-7
- [13] Ted Belytschko, Thomas J.R Hughes, "Computational methods for transient analysis", Amsterdam: North-Holland 1983, ISBN 0-444-86479-2
- [14] Ansys User's Manual for Revision 5.1 Vol I&II, Users manual, Sep 30 1994, D 9471
- [15] Ansys User's Manual for Revision 5.1 Vol IV, Theory manual, Sep 30 1994, D 9471
- [16] Jan Petersson, "Fourieranalys", Rex Offsettryck 434 97 Kungsbacka,Göteborg 1995, ISBN 992-420032-2
- [17] Lars Eldén, Linde Wittmeyer-Koch, "Numerisk analys-en intoduktion", Studentlitteratur, Lund 1996, ISBN 91-44-00172-X
- [18] Ragnar Grahn, Per-Åke Jansson: Dynamik, Studentlitteratur, Lund 1995, ISBN 91-44-48841-6
- [19] A Samuelsson, K Runesson, "Byggnadsmekanik knäckning", Studentlitteratur Lund, ISBN 91-44-37481-x
- [20] Sven Ohlsson, "Kompendium i konstruktionstecknisk dynamik, Intern, CTH Göteborg 1998
- [21] Qi-Zheng Wang, "A study of the effect of mass loading on the shock environment", Shock and Vibration Bulletin 54:th Symposium on Shock and Vibration, part 2 June 1984 USA, pp 183-191

- [22] AutoSEA©, "Reference manual and user's guide"
- [23] Claes R Fredö, "Statistical Energy Analysis and the individual case", CTH Göteborg 1995 (int) Report F 95-02, ISBN 91-7197-157-2
- [24] NAFEMS, "A Finite Element Dynamics Primer", edit by D.Hitchings, Great Britain 1992 Glasgow, ISBN 1874376 05 0, pp 70-73

## Appendix A

### The Shock Response Spectrum (SRS)

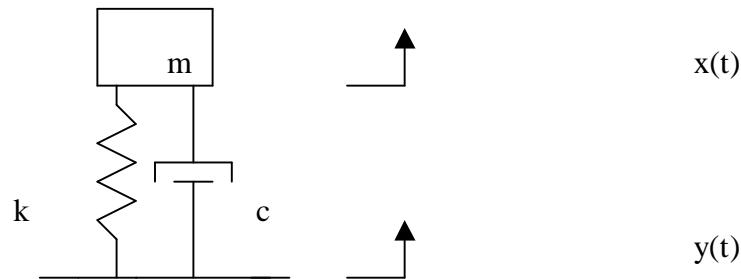


**Figure A1:** Single degree of freedom model

Newton's second law can be applied to a free-body diagram. A summation of forces yields the following governing differential equation of motion, where  $x$  is the displacement of the mass:

$$mx'' + cx' + kx = cy' + ky \quad \dots(1)$$

$y$  is an arbitrary function with the shape of a typical pyrotechnic shock pulse. The dots denotes time derivation. Assume the second derivative of  $y$  is known, then in special cases one could derive explicit solutions of  $x(t)$ . Consider a square pulse with duration  $\tau$  and amplitude  $a$ .(fig A2) This type of pulse is rear in reality but is used here as an example.

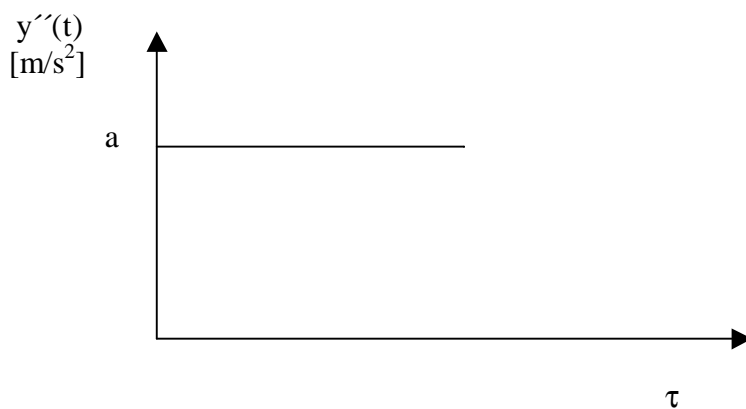


**Figure A2:** Input acceleration

The maximum acceleration of  $x''(t)$  will be calculated in the time domain for pedagogical reasons.

As  $y$  is independent of  $x$ ,  $y''(t) = a$ ;  $y(t) = at^2/2 + At + B$  together with the initial conditions  $y(0) = 0$  and  $y'(0) = 0$  gives  $y(t) = at^2/2$  and (1) can in this case be rewritten as

$$x'' + (c/m)x' + (k/m)x = (c/m)at + (k/m)at^2/2 \quad \dots(2)$$

By convention  $\omega = \sqrt{(k/m)}$  and  $\zeta = c/(2\sqrt{km})$ . Rewrite (2) as

$$x'' + 2\zeta\omega x' + \omega^2 x = 2\zeta\omega at + \omega^2 at^2/2 \quad \dots(3)$$

Mathematically, the solution consists of two parts: One homogeneous  $x_h$  and one particular part  $x_p$  [11]. In step one the homogeneous part is sought. In other words, the solution is found for  $y(t) = 0$ . Assume small damping,  $\zeta < 1$ . The homogenous solution  $x_h$  is found to be [18]: (see any mathematical handbook).

$$x_h(t) = e^{-\zeta\omega t}(A\sin(\omega d t) + B\cos(\omega d t)) \quad \dots(4)$$

where  $A$  and  $B$  are constants depending on the initial conditions and  $\omega d = \omega\sqrt{(1 - \zeta^2)}$ . The particular solution is depending on the input. Here  $x_p = at^2/2 - a/\omega^2$ . The complete expression:

$$x_{tot} = x(t) = x_h + x_p = e^{-\zeta\omega t}(A\sin(\omega d t) + B\cos(\omega d t)) + at^2/2 - a/\omega^2 \quad \dots(5)$$

The initial condition  $x(0) = 0$  and  $x'(0) = 0$  determine  $A$  and  $B$ . (5) can then be written as

$$x(t) = e^{-\zeta\omega t}[(\zeta a/\omega^2 \sin(\omega d t) + (a/\omega^2)\cos(\omega d t))] + at^2/2 - a/\omega^2 \quad \dots(6)$$

The *maximum acceleration* is sought, derivate (6) twice:

$$x''(t) = e^{-\zeta\omega t}[(\zeta^3 a \omega/\omega d) + (\zeta a \omega d/\omega)\sin(\omega d t) - (\zeta^2 a + a \omega d^2/\omega^2)\cos(\omega d t)] + a \quad \dots(7)$$

An important notation is that (6) and (7) is valid only when  $\tau > t \geq 0$ . Otherwise one have to solve the homogeneous part of (1) again with initial condition  $x_2(\tau) = x(\tau)$  and  $x_2'(\tau) = x'(\tau)$  and the particular part using the fact that  $y_2(\tau) = y(\tau)$ ,  $y_2'(\tau) = y'(\tau)$  and  $y_2'' = 0$ .

In the case of a square pulse the displacement function  $x_2(t)$  after time  $\tau$  becomes:

$$x_2(t) = e^{-\zeta\omega t}(A\sin(\omega d t) + B\cos(\omega d t)) + y'(\tau)t + y(\tau) \quad \dots(8)$$

Where  $B = x(\tau) - y(\tau)$  and  $A = (x'(\tau) + \zeta\omega[x(\tau) - y(\tau)] - y'(\tau))/\omega d$

A comonly used value of  $\zeta$  is 0.05 and  $\omega = 2\pi f$ . Let  $x''_{max} = \max(x'', x_2'')$

For the square pulse example set  $f = 1$  Hz (resonance frequency for the system =  $2\pi$ ) and  $a = 100g = 981m/s^2$ .

Then the following plots appear:

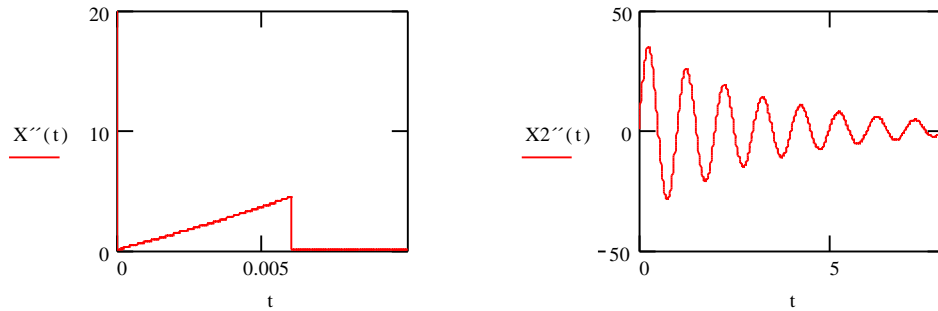


**Figure A3a,b** acceleration as function of time,  $f = 1\text{Hz}$

From figure A3b:  $x''_{\max} \approx 37\text{m/s}^2$  when  $f = 1\text{ Hz}$ . Now let  $f = 2, 3, \dots, 10\,000\text{ Hz}$  and calculate the corresponding maximum acceleration. Any arbitrary set of unique natural frequencies can be used for the shock response spectrum calculation. A typical scheme however, is based on proportional bandwidth (see maintext). By using for example Matlab or Mathcad one can calculate the maximum acceleration for every frequency. The response for  $f = 2\text{ Hz}$  is  $x_{\max 2} \approx 58\text{m/s}^2$ .

To receive the SRS, plot the  $x_{\max,i}$  against  $f_i$  on a log-log logarithmic scale. For the square pulse, the SRS plot are given below:

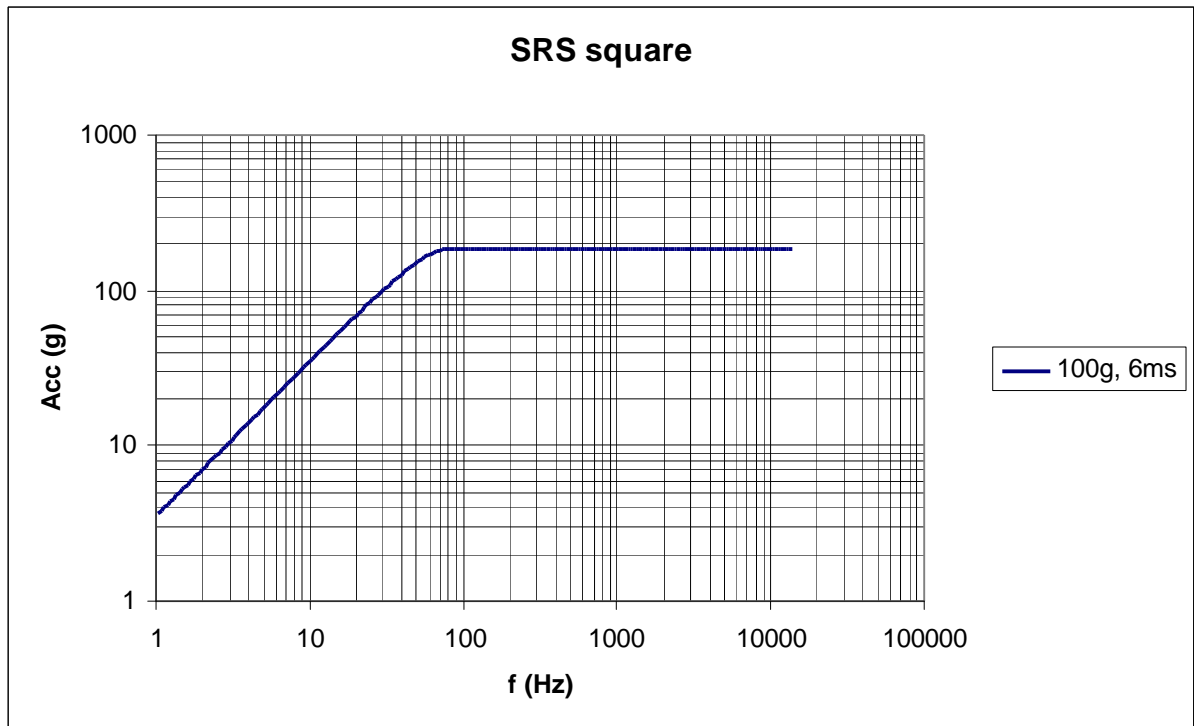


**Figure A4:** SRS of a square pulse

Usually the tolerance of the SRS is given in dB. An amplitude difference of 6 dB means that the higher amplitude is twice the lower amplitude. The difference in dB between two amplitudes A and B is calculated by [7]:

$$\Delta\text{dB} = 20\log[A/B]$$

The slope of a line on a log – log plot is given by

$$N = \log[A_2/A_1]/\log[f_2/f_1]$$

Where  $(f_1, A_1)$  and  $(f_2, A_2)$  are the two endpoint coordinates of the line.

When the input signal  $y''(t)$  has the shape of a pyrotechnical pulse, (1) can be solved using a convolution integral approach based on Laplace and Z-transforms or Fourier transforms. The differential equation from The Laplace and Z-transform is [7]:

$$x''_i = 2\exp[-\zeta\omega_n\Delta t]\cos(\omega\Delta t)x''_{i-1} - \exp[-2\zeta\omega_n\Delta t]x''_{i-2} + 2\zeta\omega_n\Delta ty''_i + \omega_n\Delta t\exp(-\zeta\omega_n\Delta t)[[(\omega_n/\omega)(1 - 2\zeta^2)]\sin(\omega\Delta t) - 2\zeta\cos(\omega\Delta t)]y''_{i-1} \dots(11)$$

Equation (11) was used to calculate the SRS of the square pulse.

The Duhamel integral, an employed finite element method or a program based on a differential equation solving algorithm such as Runge-Kutta could be used to solve the equation. See T.Irvine [6] for complete derivation of equation (11).

An important simple shock pulse is the half sine pulse. If a half sine pulse is used as input, the test is called a drop table test. When dropping an item and measuring the impact, a sinusoidal acceleration curve is received. This test has much lower acceleration input than the pyroshock test.

By Fourier transform the displacement response,  $x$ , of the mass,  $m$ , to a sinusoidal exciting motion with amplitude  $A$  can be written [16]:

$$x = H(\omega)Ae^{j\omega t} \quad \text{where } e^{j\omega t} \text{ represents the sinusoidal oscillation with period } \omega_0.$$

	Excitation quantity		
Response quality	Displacement	Velocity	Acceleration
Displacement, $x(t)$	$ H(f)  = D_1/D_2$	$ H(f)  = D_1/2\pi f D_2$	$ H(f)  = D_1/4\pi f^2 D_2$
Velocity $v(t)$	$ H(f)  = 2\pi f D_1/D_2$	$ H(f)  = D_1/D_2$	$ H(f)  = D_1/2\pi f D_2$
Acceleration $a(t)$	$ H(f)  = 4\pi f^2 D_1/D_2$	$ H(f)  = 2\pi f D_1/D_2$	$ H(f)  = D_1/D_2$

**Figure A5:** Table for simple transformation when the input is sinusoidal [12].

Where  $Q = 1/2\zeta = 1/c\sqrt{(k*m)} = \text{quality factor (see main text damping)}$ ,  $\omega_0 = 2\pi f_0$  and  $D_1 = \sqrt{[1 + (1/Q^2)(f/f_0)^2]}$ ,  $D_2 = \sqrt{[(1-(f/f_0)^2)^2 + (1/Q^2)(f/f_0)^2]}$

## Appendix B

### Explicit and implicit analysis

In this appendix we will derive one explicit and one implicit scheme and try to point out some ideas and terms connected with dynamic transient analysis.

The central difference method:

The second derivative of the displacement  $U$  with respect to  $t$  at time  $t =$

$$U''_t = (1/\Delta t^2) * [U_{t-\Delta t} - 2U_t + U_{t+\Delta t}] \quad \dots(1)$$

This is the central difference approximation of the second derivative. See [17] for a derivation of this expression.

$$U'_t = (1/2\Delta t) * [U_{t-\Delta t} + U_{t+\Delta t}] \quad \dots(2)$$

The displacement solution for time  $t+\Delta t$  is obtained by considering the equation of motion at time  $t$ , i.e:

$$MU'' + CU' + KU = R \quad \dots(3)$$

(1) and (2) yields:

$$M_t \cdot \frac{1}{\Delta t} (U_{t+\Delta t} - 2 \cdot U_t + U_{t-\Delta t}) + C_t \cdot \frac{1}{2 \cdot \Delta t} (U_{t+\Delta t} - U_{t-\Delta t}) + K_t U_t = R_t$$

Rearranging the terms:

$$\left( \frac{1}{\Delta t^2} \cdot M + \frac{1}{2 \Delta t} \right) \cdot U_{t+\Delta t} = \left[ R_t - \left( K - M \cdot \frac{2}{\Delta t^2} \right) \cdot U_t \right] + \left( C \cdot \frac{1}{2 \Delta t} - M \cdot \frac{1}{\Delta t^2} \right) \cdot U_{t-\Delta t} \quad \dots (4)$$

From which we can solve for  $U$  at time  $t+\Delta t$ . It should be noted that the solution of  $U$  at time  $t+\Delta t$  is based on the equilibrium conditions at time  $t$ ; i.e.  $U$  at  $t+\Delta t$  is calculated using (3) at time  $t$ . For this reason the integration procedure is called an explicit integration method.

An observation is that using the central difference method, the calculation of  $U$  at time  $t+\Delta t$  involves  $U$  at time  $t$  but also  $U$  at time  $t-\Delta t$ . Therefore, to calculate the solution at time  $\Delta t$ , a special starting procedure must be used [10]. Since  $U$  at  $t=0$  and  $U'$  at time  $t=0$  is known,  $U''$  at time  $t=0$  is calculated from (3). To find  $U$  at time  $-\Delta t$  one add (1) and (2):

$$2U_{-\Delta t} - 2U_0 = \Delta t^2 U''_0 - 2\Delta t U'_0 \quad \text{which yields}$$

$$U_{-\Delta t, i} = U_{0, i} - \Delta t U'_{0, i} + (\Delta t^2 / 2) U''_{0, i} \quad \dots(5)$$

Example: Solve the system below:

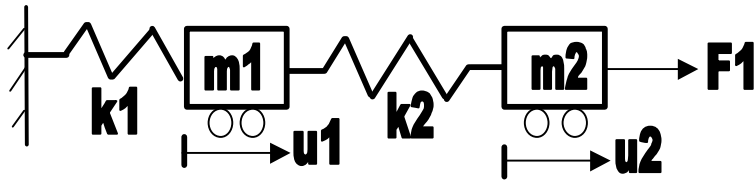


**Figure B1:** System with two degrees of freedom.

Let  $K_1 = 4$ ,  $K_2 = 2$ ,  $M_1 = 1$ ,  $M_2 = 1$ ,  $F_1 = 0$ ,  $F_2 = 10$

To find a time step, a mode superposition analyse is performed. To find the frequency of the vibration,  $\omega$  (radians/second), the system  $\det(\mathbf{K} - \omega^2\mathbf{M}) = 0$  is solved. The result is  $\omega_1 = \sqrt{2}$  and  $\omega_2 = \sqrt{5}$ . From this corresponding frequencies  $f_i$  and period time  $T_i$  can be calculated.

The smallest period  $T_2 = 1/f_2 = 1/(\omega_2/2\pi) \approx 2.81$ s. i choose a time step  $\Delta t = 0.28$ .

$$\mathbf{M} := \begin{bmatrix} 2 & 0 \\ 0 & 1 \end{bmatrix} \quad \mathbf{C} := \begin{bmatrix} 0 & 0 \\ 0 & 0 \end{bmatrix} \quad \mathbf{F} := \begin{bmatrix} 0 \\ 10 \end{bmatrix} \quad (\text{independent of } t) \quad \mathbf{K} := \begin{bmatrix} 6 & -2 \\ -2 & 4 \end{bmatrix}$$

Because no damping is included in this example, (4) reduces to

$$[\mathbf{M}/\Delta t^2]\mathbf{U}_{t+\Delta t} = \mathbf{R}_t - [\mathbf{K} - (2/\Delta t^2)\mathbf{M}]\mathbf{U}_t - [\mathbf{M}/\Delta t^2]\mathbf{U}_{t-\Delta t} \quad \dots(6)$$

Assume that  $\mathbf{U}_0 = 0$  and  $\mathbf{U}'_0 = 0$ . Then (3) becomes

$$\left[ \begin{bmatrix} 2 & 0 \\ 0 & 1 \end{bmatrix} \cdot \mathbf{U}''_0 + \begin{bmatrix} 6 & -2 \\ -2 & 4 \end{bmatrix} \cdot \begin{bmatrix} 0 \\ 10 \end{bmatrix} \right] = \begin{bmatrix} 0 \\ 10 \end{bmatrix} \quad \mathbf{U}''_0 := \begin{bmatrix} 1 & 0 \\ 0 & 2 \end{bmatrix} \cdot \begin{bmatrix} 0 \\ 10 \end{bmatrix} \cdot \frac{1}{2}$$

$$\text{so } \mathbf{U}''_0 = \begin{bmatrix} 0 \\ 10 \end{bmatrix}$$

Rewrite the terms in (6) as  $MeU_{t+\Delta t} = R_t - K1U_t - M1U_{t-\Delta t}$ . This equation is to be solved at each time step. Define some constants:

$$a0 := \frac{1}{\Delta t^2} \quad a0 = 12.755 \quad a1 := \frac{1}{2 \cdot \Delta t} \quad a1 = 1.786$$

$$a2 := 2 \cdot a0 \quad a2 = 25.51 \quad a3 := \frac{1}{a2} \quad a3 = 0.039$$

$$Me := a0 \cdot M + a1 \cdot C \quad Me = \begin{bmatrix} 25.51 & 0 \\ 0 & 12.755 \end{bmatrix} \quad M1 := a0 \cdot M - a1 \cdot C$$

$$K1 := K - a2 \cdot M \quad K1 = \begin{bmatrix} -45.02 & -2 \\ -2 & -21.51 \end{bmatrix} \quad M1 = \begin{bmatrix} 25.51 & 0 \\ 0 & 12.755 \end{bmatrix}$$

In this example  $Me$  is equal to  $M1$ , which is not normally the case. When damping is included  $Me > M1$ .

Next step is to find a starting procedure. From (5)  $U_{-\Delta t}$  and  $U_0$  calculates as:

$$U_0 := \begin{bmatrix} 0 \\ 10 \end{bmatrix} \cdot a3 \quad U_0 = \begin{bmatrix} 0 \\ 0.392 \end{bmatrix} \quad U_1 := \begin{bmatrix} 0 \\ 0 \end{bmatrix}$$

Note that the index at time  $-\Delta t$  is denoted by 0. The reason is that the mathcad procedure can fail when an index that is not an integer is used.

Following algorithm is used here:

$$U_{k+1} := Me^{-1} \cdot \left[ \begin{bmatrix} 0 \\ 10 \end{bmatrix} - K1 \cdot U_k - M1 \cdot U_{k-1} \right]$$

This algorithm gives the solution for both masses. For example at time  $k = 2\Delta t = 0.56 = k_4$ ,  $U_4$  is:

$$U_4 = \begin{bmatrix} 0.168 \\ 2.834 \end{bmatrix} \blacksquare$$

Now calculate the exact response. It is done by mode superposition analyse and the exact solution is given below (only first mass). The interested reader are exhorted to contact the author for a complete derivation:

$$Z(i) := \frac{-5}{3} \cdot \cos[\sqrt{2} \cdot (0.28(i-1))] + 1 - \frac{-2 \cdot [\cos[\sqrt{5} \cdot (0.28(i-1))]]}{3}$$

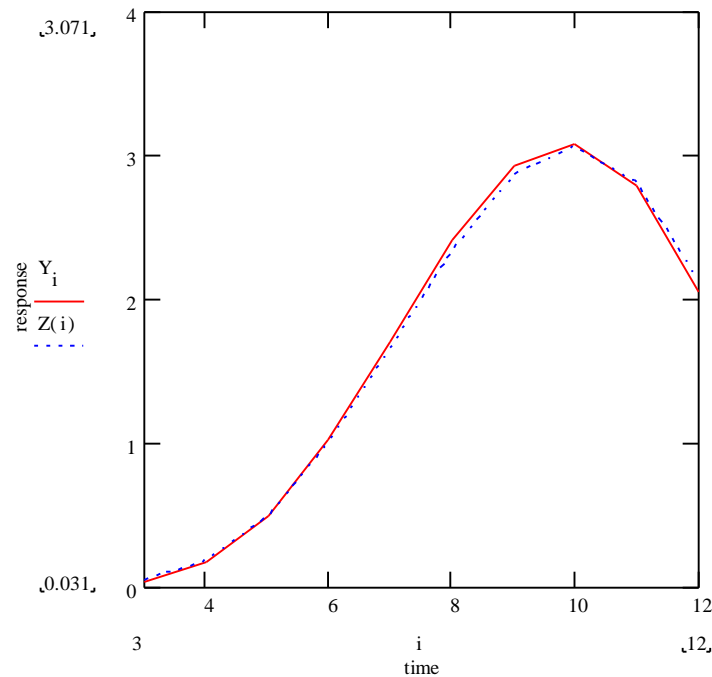


**Figure B2:** Exact and approximate solution of the example.

The numerical result listed together with the results from the explicit analysis and the exact solution.

Now consider  $\Delta t = 28$  s. Following through the same calculation, one find that  $U_{\Delta t} = [0, 3.83 \cdot 10^3]$  and  $U_{2\Delta t} = [3.03 \cdot 10^6, -1.27 \cdot 10^7]$ , and the displacement continues to increase due to the large time step. One can not expect any accuracy, but the never-ending increase in this example is a consequence of the time integration scheme not being stable, it is only *conditionally* stable. One can show that for stability one need  $\Delta t_{cr} \leq (1/\pi)T_{min}$  where  $T_{min}$  is calculated by norms, special techniques or as here by a simple mode superposition analyses.  $\Delta t_{cr} = 2.8/\pi = 0.89$  s.

### The Houbolt method

Consider the backward difference estimation with wrong of order  $\Delta t^2$  [17]:

$$U'_{t+\Delta t} = (1/6\Delta t)[11U_{t+\Delta t} - 18U_t + 9U_{t-\Delta t} - 2U_{t-2\Delta t}] \quad \dots(7)$$

$$U''_{t+\Delta t} = (1/\Delta t^2)[2U_{t+\Delta t} - 5U_t + 4U_{t-\Delta t} - U_{t-2\Delta t}] \quad \dots(8)$$

Recall the equation of motion at time t:

$$MU''_t + CU'_t + KU_t = R_t \text{ now consider } t = t + \Delta t.$$

$$\Rightarrow MU''_{t+\Delta t} + CU'_{t+\Delta t} + KU_{t+\Delta t} = R_{t+\Delta t} \quad \dots(9)$$

Use of (7) and (8) in (9) yields:

$$M(1/\Delta t^2)[2U_{t+\Delta t} - 5U_t + 4U_{t-\Delta t} - U_{t-2\Delta t}] + C(1/6\Delta t)[11U_{t+\Delta t} - 18U_t + 9U_{t-\Delta t} - 2U_{t-2\Delta t}] + KU_{t+\Delta t} = R_{t+\Delta t}$$

Rearrange the terms:

$$[2M/\Delta t^2 + 11C/6\Delta t + K]U_{t+\Delta t} = R_{t+\Delta t} + [5M/\Delta t^2 + 3C/\Delta t]U_t - [4M/\Delta t^2 + 3C/2\Delta t]U_{t-\Delta t} + [M/\Delta t^2 + C/3\Delta t]U_{t-2\Delta t} \quad \dots(10)$$

Note that the term  $KU_{t+\Delta t}$  appears because (9) is considered at time  $t + \Delta t$  and not at time  $t$  as in the central difference method. The Houbolt method is, for this reason, an implicit integration scheme [10].

Also note that if one choose  $M = C = 0$ , (10) becomes

$$\begin{bmatrix} 6 & -2 \\ -2 & 4 \end{bmatrix} \cdot U = \begin{bmatrix} 0 \\ 10 \end{bmatrix} \quad U := \frac{1}{20} \cdot \begin{bmatrix} 4 & 2 \\ 2 & 6 \end{bmatrix} \cdot \begin{bmatrix} 0 \\ 10 \end{bmatrix} \quad U = \begin{bmatrix} 1 \\ 3 \end{bmatrix}$$

This is the static solution of the problem. In the explicit case no valuable information is obtained.

Because no damping is included in the example, (10) reduces to

$$[M(2/\Delta t^2) + K]U_{t+\Delta t} = R_{t+\Delta t} + [5M/\Delta t^2]U_t - [4M/\Delta t^2]U_{t-\Delta t} + [M/\Delta t^2]U_{t-2\Delta t}$$

We note that the solution of  $U_{t+\Delta t}$  requires knowledge of  $U_t$ ,  $U_{t-\Delta t}$ ,  $U_{t-2\Delta t}$ . Although the knowledge of  $U_0$ ,  $U'_0$ , and  $U''_0$  is useful to start the integration scheme, it's more accurate to calculate  $U_{\Delta t}$  and  $U_{2\Delta t}$  by some other means. A special starting procedure is usually employed.

One way of proceeding is to integrate (3) for the solution of  $U_{\Delta t}$  and  $U_{2\Delta t}$  using a different integration scheme, possibly a conditionally stable method. Here the result from the explicit scheme is used.

$$U_1 := \begin{bmatrix} 0 \\ 0.392 \end{bmatrix} \quad U_2 := \begin{bmatrix} 0.030733 \\ 1.44507 \end{bmatrix} \quad U_0 := \begin{bmatrix} 0 \\ 0 \end{bmatrix}$$

Define some constants for the calculation:

$$\Delta t := 0.28 \quad a_0 := \frac{2}{\Delta t^2} \quad a_1 := \frac{11}{6 \cdot \Delta t} \quad a_2 := \frac{5}{\Delta t^2} \quad a_3 := \frac{3}{\Delta t} \quad a_4 := -2 \cdot a_0 \quad a_5 := \frac{-a_3}{2}$$

$$a_6 := \frac{a_0}{2} \quad a_7 := \frac{a_3}{9} \quad i := 0..7 \quad a^T = (25.51 \ 6.548 \ 63.776 \ 10.714 \ -51.02 \ -5.357 \ 12.755 \ 1.19)$$

Calculate the term in front of  $U_{t+\Delta t}$ ,  $K_s$ .  $K$  is used without index in the calculation.

$$K := \begin{bmatrix} 6 & -2 \\ -2 & 4 \end{bmatrix} + a_0 \cdot \begin{bmatrix} 2 & 0 \\ 0 & 1 \end{bmatrix} \quad K = \begin{bmatrix} 57.02 & -2 \\ -2 & 29.51 \end{bmatrix}$$

For each time step one need  $R_{t+\Delta t}$  which in this case is:

$$R_{k+1} = \begin{bmatrix} 0 \\ 10 \end{bmatrix} + \begin{bmatrix} 2 & 0 \\ 0 & 1 \end{bmatrix} \cdot (a_2 \cdot U_k - a_4 \cdot U_{k-1} + a_6 \cdot U_{k-2}) \quad \text{Solving } KU_{t+\Delta t} = R_{t+\Delta t} \text{ for 12 steps:}$$

$$U_{k+1} := K^{-1} \cdot \left[ \begin{bmatrix} 0 \\ 10 \end{bmatrix} + \begin{bmatrix} 2 & 0 \\ 0 & 1 \end{bmatrix} \cdot (a_2 \cdot U_k + a_4 \cdot U_{k-1} + a_6 \cdot U_{k-2}) \right]$$

$$V_k := \left| \left( U_k^T \right)^{<0>} \right|$$

The last row reads a vector for the plot.

Note that  $V_i$  is the displacement of the first mass considered in the problem and thus  $V_i$  = the first row of  $U_i$ .

Now plot the displacement  $V$ s time:

For example:

$$V_4 = 0.461 \quad Q_3 = 0.999$$

$$V_5 = 0.923 \quad Q_4 = 1.002$$

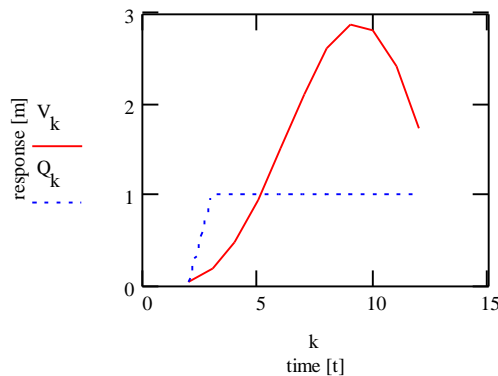


**Figure B3:** Implicit plots with different  $\Delta t$ .

Where  $Q$  is the solution with time step  $\Delta t = 28$  s

The numerical result is presented in table A1 together with the explicit scheme and the exact solution.

Observe the unconditional stability of the Houbolt method and that the static solution of the problem is:

$$\begin{bmatrix} 6 & -2 \\ -2 & 4 \end{bmatrix} \cdot \begin{bmatrix} U_1 \\ U_2 \end{bmatrix} = \begin{bmatrix} 0 \\ 10 \end{bmatrix} \quad \text{which yields} \quad \begin{bmatrix} U_1 \\ U_2 \end{bmatrix} = \begin{bmatrix} 1.0 \\ 3.0 \end{bmatrix}$$

The Houbolt method is thus producing the static solution when  $\Delta t$  is chosen too large or if the mass and damping effects are neglected. Other implicit schemes are Wilson  $\theta$  and Newmark method.

The response of unconditionally stable methods such as Houbolt, Wilson  $\theta$  and Newmark is very inaccurate when a too large time step is chosen, but the values do not increase in the same way as in the conditionally stable case.

Time	$\Delta t$	$2\Delta t$	$3\Delta t$	$4\Delta t$	$5\Delta t$	$6\Delta t$	$7\Delta t$	$8\Delta t$	$9\Delta t$	$10\Delta t$	$11\Delta t$	$12\Delta t$
Central-difference.	0	0.0307	0.168	0.487	1.02	1.70	2.40	2.91	3.07	2.77	2.04	1.02
Houbolt	0	0.0307	0.167	0.461	0.923	1.50	2.11	2.60	2.86	2.80	2.40	1.72
Exact solution	0.003	0.038	0.176	0.486	0.996	1.66	2.338	2.861	3.052	2.806	2.131	1.157
Houbolt $\Delta t=28s$	0	0.0307	0.999	0.999	1	1	1	1	1	1	1	1
C.D with $\Delta t=28s$	0	303000	Increasing $\rightarrow$									

**Figure B4:** Numerical results from the example (only  $U_1$ ).

## Appendix C

### Exact solution of free vibration of a rectangular plate

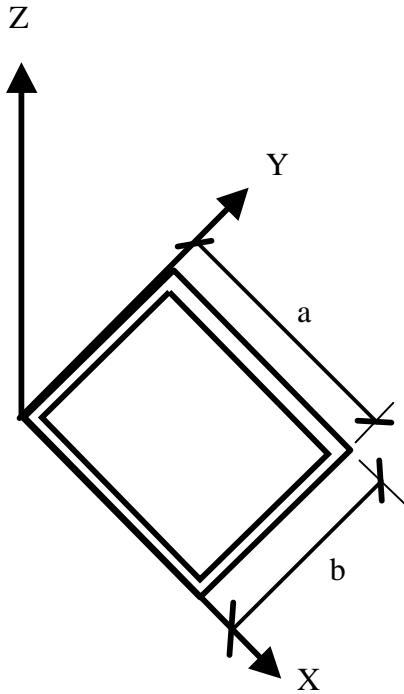


**Figure C1:** Simple supported plate with coordinate axis.

The differential equation of a thin plate, with axis as in fig C1, is given by [20]:

$$D \left( \frac{d^4}{dx^4} \cdot \omega + 2 \cdot \frac{d^4}{dx^2 dy^2} \cdot \omega + \frac{d^4}{dy^4} \cdot \omega \right) = q(x, y)$$

Where  $\omega$  is the displacement in the z-direction and  $q(x,y)$  is the intensity of loading normal to the surface of the plate.  $D$  is the flexural stiffness given by:

$$D = \frac{Et^3}{12(1-\nu^2)}$$

Where  $t$  is the thickness of the plate and  $\nu$  is Poisson's ratio. Free vibration and ignored damping means that only inertia forces need to be considered. If  $m$  is the mass/unit area of the plate,  $q(x,y,t)$  becomes

$$q(x, y, t) = -m \frac{d^2}{dt^2} \omega$$

and

$$D \left( \frac{d^4}{dx^4} \cdot \omega + 2 \cdot \frac{d^4}{dx^2 dy^2} \cdot \omega + \frac{d^4}{dy^4} \cdot \omega \right) + m \cdot \frac{d^2}{dt^2} \omega = q(x, y) \quad \dots (1)$$

By the method of separation of variables the transverse displacement can be calculated as  $\omega(x, y, t) = \phi(x, y) \cdot Y(t)$  [1]. This substitution yields:

$$Y''(t) + \omega^2 Y(t) = 0 \quad \text{and}$$

$$D \left( \frac{d^4}{dx^4} \cdot \phi(x, y) + 2 \cdot \frac{d^4}{dx^2 dy^2} \cdot \phi(x, y) + \frac{d^4}{dy^4} \cdot \phi(x, y) \right) + m \cdot \frac{d^2}{dt^2} \phi(x, y) = \alpha^4 \cdot \phi(x, y) \quad \dots (2)$$

Where  $\alpha^4 = m\omega^2/D$

In the case of rectangular plates, the displacement function:

$$\phi(x, y) = \sin(r\pi x/a) \sin(s\pi y/b) \quad \dots (3)$$

where  $r$  and  $s$  are integers  $> 0$ , satisfies the boundary conditions for simply supports of all edges. The boundary conditions are[19]:

$$(\phi)_{x=0, a} = (\phi)_{y=0, b} = (d^2/dx^2)_{x=0, a} = (d^2/dy^2)_{y=0, b} = 0$$

in the case of rectangular plate. By substituting (3) into (2) one finds that

$\alpha^2 = \pi^2(r^2/a^2 + s^2/b^2)\sqrt{D/m}$  or  $\omega\sqrt{(m/D)} = \pi^2(r^2/a^2 + s^2/b^2)$  which yields

$$\omega = \pi^2 \left( \frac{r^2}{a^2} + \frac{s^2}{b^2} \right) \cdot \sqrt{\frac{D}{m}}$$

The lowest natural frequency will occur when  $r = s = 1$  and the corresponding mode shape will be a half sine curve in both  $x$  and  $y$  directions.

The next two natural frequencies will occur when either  $r$  or  $s$  is increased to 2 and the other remains unchanged. This will have the effect of making a half sine curve in one direction and a full sine curve in the other.

## Appendix D

### User's manual for pyroshock measurements

#### 1. Impact

The hammer give the fixture a impact. The accelerometer amplitude-time signal shows in the oscilloscope window.

#### 2. Transfer of the amplitude-time signal to the PC

In the HP-VEE outfile part, you decide which PC folder you would like to place your oscilloscope outfile into. We use the folder **C:/exjobbpyro/srs**. The outfiles are named **accs.lc1**, **accs.lc2**, **accs.lc3** and **accs.lc4** depending on which channel you wish to save. In the window *For Range* you chose which channel on the oscilloscope that will be transferred.

#### 3. Scangraph

Scangraph is a matlab program which convert the oscilloscope graph to an amplitude-time vectorfile.

To success you must be in current directory. In our case **c:/exjobbpyro/srs**.

In matlab you get this directory then you write: **cd c:/exjobbpyro/srs**. To call the program you type: **scangraph('accs.lc1', accs.txt)**; There the first part is the outfile from the oscilloscope and the second one the resulting amplitude-vectorfile in text format.

#### 4. SRS-program

The most widely used technique for qualifying pyroshock is the Shock Response Spectrum (SRS). The SRS is a method of reducing the time-history to compare shocks motions, to design equipment to withstand shocks, or to formulate laboratory test simulating environmental condition.

We used a SRS program **qsrs.cpp** developed by Tom Irwine. You transfer the scangraph outfile: **accs.txt** into this program. The program asking for damping factor. You normally type 5% here. The qsrs.cpp program has a starting frequency in 5 Hz. The ending frequency is equal to the sampling rate divided by 8. The frequency spacing is 1/12 octave.

The outfiles you will get are:

- **srs.out**, this is a text output file which containing natural frequency with there positive and negative acceleration (G).
- **srs.grp** and **srs2.grp** are the graph file. To use them you must have a special graph program. We haven't this so we do our graph in Excel with srs.out file.

## 5. Excel

We open here the **srs.out** file. You must do some step in ‘Text Import Wizard’:

1. You choose delimited, which is the file type that best describes your data. Click on Next.
2. In step 2 you choose tab and Space, then click Next.
3. In step 3 you accept the general data form and click ‘Finished’.
4. Now have you get the information in Excel window (table\_).

Some transfer faultation have been here. The only information you interested in are shown in the three first column(I have **bold** marking them). The first one show the natural freuency **fn(Hz)**. The second one the peak positive accleration **pos**. The third is named **srs(G)** this is instead the peak negative acceleration **neg**.

SHOCK	RESPONSE	SPECTRUM	OUTPUT					
damp=0.04								
dt=1e-006	sec	sr=1e+006	samples/sec					
total	samples=100002							
duration=0.100002	sec							
start	time=0.000000	sec						
end	time=0.100001	sec						
<b>fn(Hz)</b>	<b>pos</b>	<b>srs(G)</b>	neg	srs(G)	pos	time(sec)	neg	time(sec)
<b>5.0</b>	<b>0.00073</b>	<b>-0.0461</b>	0.00813	0.1				
<b>5.3</b>	<b>0.00080</b>	<b>-0.0466</b>	0.00813	0.1				
<b>5.6</b>	<b>0.00089</b>	<b>-0.0468</b>	0.00813	0.09346				
<b>The last three rows</b>								
<b>115852.</b>	<b>3.5</b>	<b>-2.5</b>	4.0E-06	9.0E-06				
<b>122741.</b>	<b>3.61</b>	<b>-2.41</b>	3.0E-06	8.0E-06				
<b>130039.</b>	<b>3.69</b>	<b>-2.17</b>	3.0E-06	0.00044				

Table\_ The Excel file srs.out

5. To plot the SRS graph you marking now the three column. Now you replace the dot with the comma. (The Excel couldn't work with dot) You find replace in the Edit menu.
6. To check the measurements quality you plot the absolute positive and negative acceleration together. Delete just the minus sign in the neg srs column.
7. You must also correct the acceleration value with a factor 100 or 1000 depending on the setting on Beran amplifier.
8. You marking now the three column and click on chart wizard here you choose XY(chatter) and the line model.
9. The last step is to change to an logarithmic scale. You do it with clicking on the axes.